Energy & Environmental Science

ROYAL SOCIETY OF CHEMISTRY

REVIEW

View Article Online
View Journal | View Issue

Cite this: *Energy Environ. Sci.*, 2026, **19**, 11

Towards inline ultrasonic characterisation of battery slurry mixing: opportunities, challenges, and perspectives

Yifei Yang,[a] Zhenyu Guo,[b] Yun Zhao,[a] Haobo Dong,[c] Maria-Magdalena Titirici,[b] Frederic Cegla,[a] Valerie Pinfield[d] and Bo Lan*[a]

Received 24th June 2025,
Accepted 25th November 2025

DOI: 10.1039/d5ee03563e

rsc.li/ees

Inefficiencies in the slurry mixing stage are a major factor in high scrap rates in battery manufacturing, thus hindering sustainable production. Current offline characterisation techniques for slurry microstructure and rheology are slow and inadequate for closed-loop quality control or process optimisation. This review evaluates ultrasound as a promising inline, non-invasive characterisation tool to address this crucial need. We critically examine decades of developments and applications in ultrasonic evaluation techniques, assessing their relevance and identifying challenges specific to the high-concentration, non-Newtonian battery slurries. Key wave-slurry interaction mechanisms, including attenuation, wave speed, scattering, and guided wave propagation, are discussed in the context of characterising microstructural features (*e.g.* particle dispersion and agglomeration) and macroscopic rheological properties (*e.g.* viscosity and viscoelasticity). To make full use of the crucial yet limited information accessible *via* ultrasound, we propose a hybrid framework marrying ultrasonic and other offline data through physics-informed machine learning for accurate and comprehensive property estimation. With the analyses and framework, this review points to a clear path towards achieving robust inline monitoring and efficient optimisation of battery slurry mixing.

Broader context

As the world transits to electrified transport and renewable energy systems, batteries have become a pillar of decarbonisation. However, underneath this rapid growth lies a less visible problem: battery manufacturing is hindered by inefficiencies, with scrap rates in gigafactories exceedingly high. These inefficiencies not only drive up costs but also undermine the environmental gains of clean energy technologies, by wasting critical materials and energy during production. One of the key contributors to this issue is electrode slurry mixing, a foundational step that determines the structural and functional quality of battery electrodes. Despite its significance, the optimisation of slurry mixing remains largely empirical, relying more on iterative trial-and-error from offline characterisations, instead of precise, real-time feedback and control guided by physics or monitoring data. Addressing this problem is vital for reducing industrial waste and increasing the reliability and affordability of battery technologies. This review makes the case for inline ultrasonic characterisation tools – combined with physics-informed predictive modelling – to transform how battery slurries are evaluated and controlled. By advancing this field, we contribute to a more sustainable, resource-efficient energy storage ecosystem that can meet the urgent demands of the environmental and climate crisis.

1 Introduction

In our society's transition to clean energy, batteries are playing a crucial role across sectors, with prominent examples including the electrification of vehicles and transportation,[1–3] and the grid-scale energy storage[4] for stabilising intermittent renewable sources (*e.g.* solar and wind[5]). These vital applications spur phenomenal demand for batteries. The most widely used type, Li-ion batteries (LIBs),[6–9] are projected to grow 27% annually and reach manufacturing capacity of 4.7 to 6.8 TWh by 2030[10,11] (Fig. 1(a)), with an estimated market value of >$400 billion.[10] Zinc- and sodium-ion batteries are also expected to grow significantly to reach respective market caps of $14.23[12] and $1.84 billion[13] by then. However, the rapidly expanding manufacturing capacity is known to suffer from high scrap rates: the manufacturing of LIB, which is more established than other battery chemistries, have typically 15–30% scrap rates in new gigafactories and ~10% even

[a] *Department of Mechanical Engineering, Imperial College London, SW7 2AZ, UK. E-mail: bo.lan@imperial.ac.uk*
[b] *Department of Chemical Engineering, Imperial College London, SW7 2AZ, UK*
[c] *School of Future Technology, South China University of Technology, China*
[d] *Chemical Engineering Department, Loughborough University, Loughborough LE11 3TU, UK*

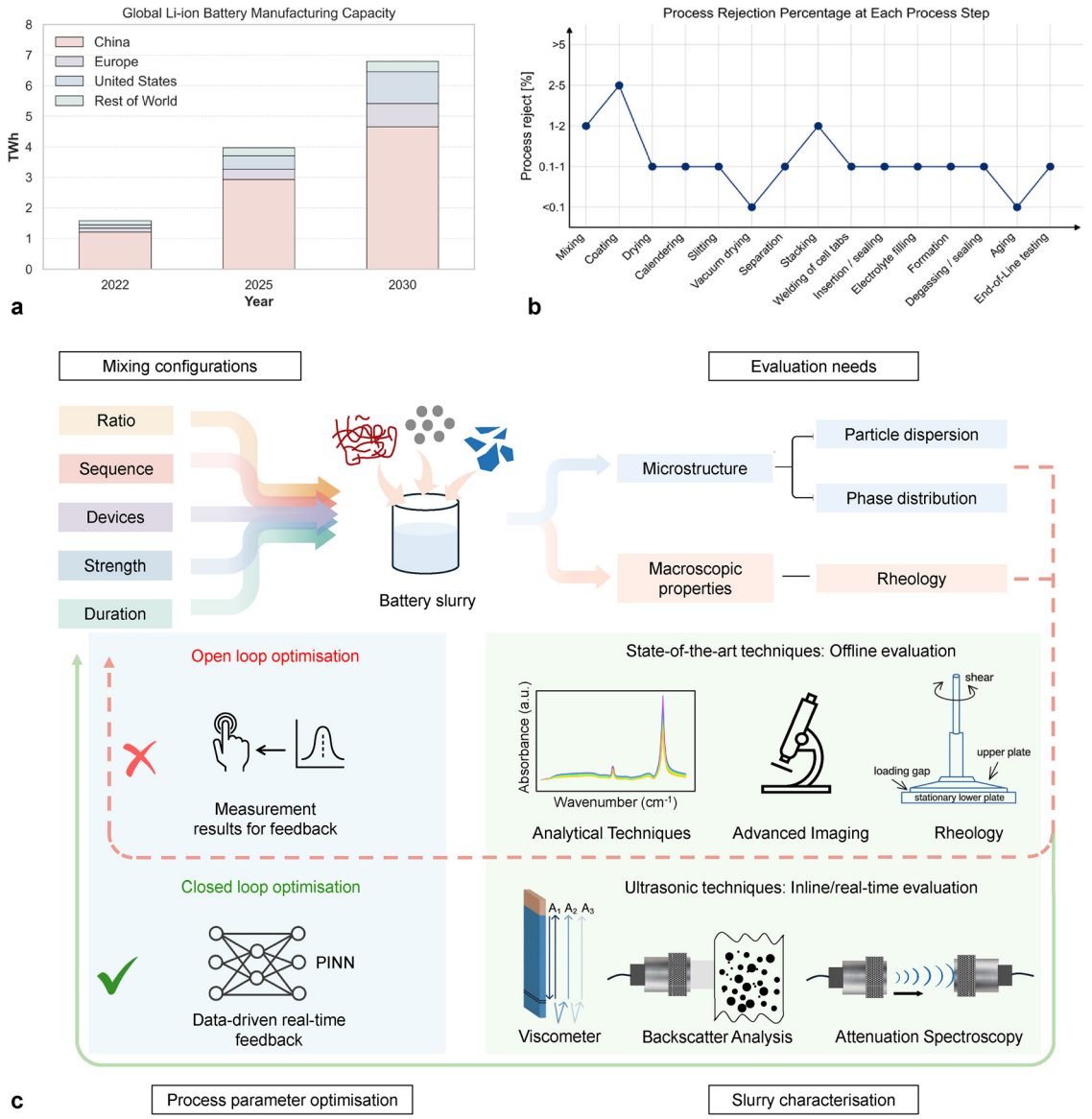

Fig. 1 (a) Expected rapid growths in global Li-ion battery manufacturing capacity. Data sourced from International Energy Agency (IEA), World Energy Investment 2023 – Overview and Key Findings,[11] accessed 24 April 2025; (b) rejection rates across all manufacturing process. Replotted from data reported in ref. 25, licensed under CC BY-NC-ND 4.0, no changes were made to the original data; (c) the overall scope of this article: to illustrate how mixing configurations influence slurry properties, and how current open-loop optimisation – which relies on offline evaluations – can be improved by a closed-loop approach with inline ultrasonic characterisation.

after five years.[14–16] The scraped materials have significant accumulated values from their manufacturing histories – the cathode of LIBs also contains precious metals (*e.g.* cobalt) which cause environmental and societal issues to mine[17–19] – and will require further investments to recycle, which makes the scrap highly costly.[20–22] Each scrap percentage is estimated to cost $32 500 per day and $10.8 M per year for just one 40-GWh factory.[15] Therefore, improving battery manufacturing efficiency and reducing the scrap rates have substantial economical and environmental impacts.[23,24]

One battery manufacturing stage that has a critical influence on the overall scrap rate is slurry mixing – the very first step in electrode production. The rejection rate of slurry mixing itself is 1–2%, the second highest across all manufacturing steps;[25] the slurry product also heavily impacts the coating process,[26] which has the highest scrap rate at ~5%,[25,27] see Fig. 1(b). In addition, the microstructures of the slurry has a deterministic influence on the finished electrode morphologies and the ultimate performance of the battery cells.[28,29] Therefore, precise and efficient characterisation of the slurry properties is a vital requirement,[30] not only to ensure the quality of electrodes and cells, but also to improve economic saving – by rejecting flawed products early and preventing them from advancing through the downstream processes. An ideal characterisation technique should also allow easy integration to the production line, to achieve real-time, dynamic, and closed-loop optimisation of manufacturing configurations.

Unfortunately, existing characterisation techniques are inadequate for such inspection requirements. This is largely due to the inherent complexities of battery slurries, which stem from multi-scale particulate interactions[31] and the myriad of parameters affecting slurry microstructure formation.[32] As a result, a range of characterisation and modelling techniques often have to be employed in tandem, with each of them characterising one aspect of the slurry properties. Examples include advanced imaging techniques (*e.g.* scanning electron microscopy, SEM or cryo-SEM) for particle sizes,[33–35] rheometers for viscosity,[36] and oscillatory shear tests for viscoelasticity.[37] However, most of these tests are expensive (require sophisticated equipment[38]) and time-consuming (conducted offline) to perform, and the aggregation of measurement results to inform configuration optimisation is complex and empirical. Consequently, the control and optimisation of the slurry mixing process is highly inefficient and complicated, ultimately contributing to persistently high scrap rates.

In this review paper, we present low-power ultrasound as a strong prospect to provide inline characterisation of battery slurry mixing. Ultrasound, being a mechanical wave, is perturbed by the slurry medium (especially the suspended particles) as it propagates, leading to quantifiable changes in wave behaviours, which provides the physical foundation for the inverse characterisation of the slurry properties.[39,40] This is pursued in decades of developments and a rich body of work,[40–47] which have established rigorous theoretical frameworks and experimental capabilities to evaluate slurry microstructures (*e.g.* particle size distribution) and macroscopic properties (*e.g.* viscosity).[39,40,48,49] As a result, ultrasonic techniques have enjoyed wide employment for the characterisation of different colloidal dispersion systems across mineral & mining,[50,51] food,[52,53] and pharmaceutical[54,55] industries. Practically, ultrasound's advantages include the abilities to penetrate optically opaque systems, to operate across length scales, and to be implemented inline with real-time responses – all of which are highly desirable for monitoring battery slurry mixing.

To replicate such successes, however, is not without its challenges. For instances, the solid concentration in battery slurries are much higher[56] than the other typical slurry systems; the suspended particles consist of multiple materials, *e.g.* soluble binder adsorbed on particle surface rather than having a clear solid–liquid boundary;[57,58] the non-Newtonian continuous (fluid) phase presents difficulties both for experiments[59] and the inverse quantification of properties such as viscosity.[60] We identify comprehensive lists of such research gaps and point out directions to potentially overcome them. One potentially winning strategy, as will be discussed in Section 5, could be to combine the information accessible by ultrasound with predictive modelling, especially the emerging physics-informed machine learning (PIML) frameworks,[61] which offers a powerful platform to incorporate not only the physical layers of ultrasonic interactions with slurries, but also the offline characterisation techniques, thus enabling a holistic estimation of slurry microstructures and macroscopic rheological behaviours.

The overarching objective of this paper is, as plotted in Fig. 1(c), to examine the unfulfilled needs for closed-loop control of slurry mixing, and to propose ultrasound as a potential solution. Note that throughout this paper, we use LIBs as examples given their prominence, but the fundamental principles of ultrasonic characterisation are general and equally applicable to slurries in other systems, such as zinc- or sodium-ion batteries and the next-generation, colloidal ink-based solar panels (*e.g.* quantum dot[62] and perovskite[63]), despite their different chemistries and particle sizes. The sections are structured to serve the purpose: Section 2 examines the slurry mixing process, with special focus on the important microstructure and properties of slurries that require characterisation. Next, we review the current state-of-the-art characterisation and modelling tools and point out their advantages and shortcomings. Section 4 then provides a general introduction to ultrasonic-based characterisation techniques, which spans from particle sizing from bulk wave attenuation to viscosity measurement from guided waves. Finally, we identify the research gaps to shifting existing knowledge within the ultrasonic field towards battery slurry evaluation, and discuss the potential directions to address them.

2 Battery slurry properties and mixing configurations

Slurry-based wet processing is the dominant method for manufacturing LIB electrodes.[64] It involves mixing and dispersing active material (AM) particles, polymer binders, and conductive additives (CA, most commonly carbon black) in a suitable solvent to produce a homogeneous slurry. Anode slurries are often aqueous,[65] with graphite as the AM,[7,66] and a combination of carboxymethyl cellulose (CMC) and styrene-butadiene rubber (SBR) as the binder;[67] whereas in cathode slurries, the solvent is typically an organic compound like *N*-methyl-2-pyrrolidone (NMP),[65] AMs lithium metal oxides (*e.g.* lithium cobalt oxide (LCO)[6,68] or lithium nickel cobalt manganese oxide (NMC)[7,69]), and the binder polyvinylidene fluoride (PVDF).[70] Before mixing, binders are usually pre-dissolved in the solvent to form a continuous phase that supports the dispersion of AM and CA particles added subsequently. Each constituent plays a critical role: the AM particles govern capacity, the CA ensures electron transport, and the binder ensures mechanical integrity and adhesion to the current collector.

As the initial step in battery manufacturing, the mixing process must produce a well-formulated dispersion that facilitates downstream fabrication stages and ultimately ensures the functional performance of the cell. To achieve these, the slurries have to meet stringent requirements in terms of microstructures at the particles scale, as well as rheological properties at the bulk scale.

2.1 Key slurry property requirements

2.1.1 Microscopic – particle dispersion, homogeneity and binder distribution. The ideal state of a battery slurry, regardless of the AM particles (*e.g.* NMC *vs.* graphite) or the binder (*e.g.* PVDF *vs.* CMC/SBR), is a homogeneous dispersion of particles, with minimal presence of aggregates or agglomerations.[71] Achieving this state requires overcoming inherent inter-particle forces[68] with sufficient energy during mixing and stabilising the dispersion afterwards.[72,73] The polymer binders should be evenly spread over AM particle surfaces, effectively acting as both an

adhesive glue and a cohesive network that ties the CA particles to the AM,[28] as depicted in Fig. 2(a). This state allows AM particles in the electrode to have maximum accessibility to Li^+ ions in electrolyte, and the diaphanous percolated CA network ensures efficient electron transportation,[28] as shown in Fig. 2(b). Metrics related to particle dispersion and distribution can therefore be derived from this ideal state to indicate the slurry quality.

Slurry dispersion is commonly evaluated using particle size distribution (PSD). A good slurry typically exhibits a narrow peak centred around the median particle size. It is interdependent with spatial homogeneity: a broader PSD may arise from increased polydispersity in insufficiently mixed slurries, due to the presence of both small aggregates (*e.g.* of CA particles) and large clusters (*e.g.* of AM agglomerations),[74] see Fig. 2(c). Poorly dispersed slurries can lead to electrode coating with uneven spread of particles and exceedingly high localised packing density (Fig. 2(d)), increasing the overall tortuosity and limiting high-rate performances.[75,76] The localised clusters also increase the likelihood of defects, which accelerate capacity fading and mechanical degradation during cycling.[77]

The distribution and morphology of binder and CA around the AM particles is collectively referred to as the carbon/binder domain (CBD).[29] In a properly formed CBD, the polymer chains adsorb onto AM particle surfaces, and their dangling ends form entangled networks with the CA particles, known as bridging flocculation,[78] which stabilise the dispersion.[79] The structure of the CBD directly impacts the slurry's macroscopic rheology,[80] the drying efficiency of the coated film[81] and performance of the electrode.[82] Achieving this optimal microstructure consistently presents a challenge, as it is highly sensitive to the mixing parameters[29] and notoriously difficult to evaluate *in situ*,[83] which is a motivation for the development of advanced characterisation techniques such as ultrasound.

In addition, chemical interfacial interactions play an important role in stabilising the suspension and influencing agglomeration at molecular scales. One way to describe these interactions is through zeta potential, which is a physical property measuring the electrostatic charge on the surface of the dispersed particles. A higher magnitude of zeta potential – positive or negative – generally indicates stronger electrostatic repulsion between particles and therefore a more stable slurry.[84] Practically, there may also exist microscopic metal particle contaminations due to equipment-wear,[85] though they are less common in stable industrial manufacturing.

2.1.2 Macroscopic – rheology. Rheology describes the flow and deformation behaviour of the slurry in response to external stresses. These properties dictate the processability of the slurry, particularly the coating process which subjects the slurry to significant shear and extensional deformation.[80] LIB slurries are typically non-Newtonian fluids, and their complex rheological behaviour reflects the interplay between the multi-scale, complex microstructures of suspended particle networks and polymer binders, which could rearrange, relax or break down under stress.[80,86]

Viscosity measures a fluid's resistance to deformation under an applied shear stress. Most LIB slurries are exhibit shear thinning, where viscosity decreases as the applied shear rate increases.[32] This behaviour is highly desirable: at low shear rates, high viscosity helps maintain particle dispersion and microstructural stability.[32] Whereas at high shear rates, particularly during slot-die or blade coating, a low viscosity is crucial for ensuring smooth, uniform film formation, reducing edge defects and enabling efficient roll-to-roll manufacturing. The transition between the viscosity regimes is fundamentally governed by the shear-induced alignment of particles and weakly aggregated networks within the slurry.[87]

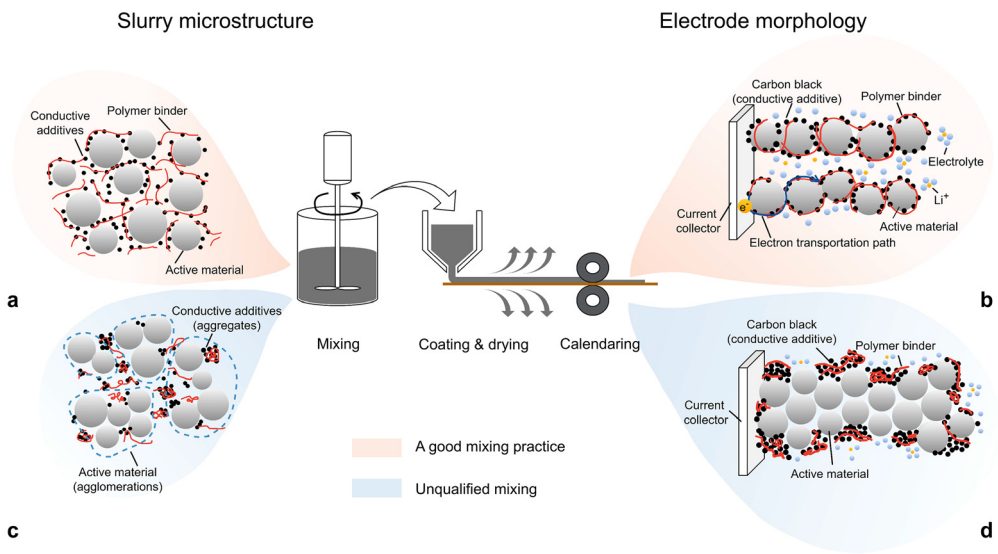

Fig. 2 Schematics of LIB-electrode slurry microstructures and resultant electrode morphologies. A desirable slurry microstructure with uniformly dispersed particles and localised percolated networks (a) tends to form a favourable electrode morphology (b)[28] while a poorly mixed slurry containing small aggregates and large agglomerations (c) normally leads to electrodes with blocked pathways for ion and electron transportation (d).[28]

Thixotropy, which describes the time-dependent viscosity reduction under constant shear stress, and the gradual recovery upon stress removal, is also commonly observed.[88] Under sustained shear of the coating process, the reduced viscosity aids application; when the shear stops, the time-dependent recovery to high viscosity is crucial for preventing excessive post-coating flow or sagging and maintaining dimensional stability.[37] Thixotropy originates from the reversible breakdown and reformation kinetics of the internal particle and binder networks.[37,80,88]

Viscoelasticity and yield stress are two additional key rheological properties, particularly important at low or intermediate stress levels.[37,86] Viscoelasticity refers to the viscous (liquid-like, dissipating mechanical energy) and elastic (solid-like, storing mechanical energy) behaviour of the slurry under deformation, which is quantified by frequency-dependent storage (G') and loss (G'') moduli,[37,89] respectively. Viscoelasticity reflects the strength and relaxation dynamics of the internal network structure.[89] A suitable level of elasticity is required to maintain suspension stability, and prevent defects like cracking or delamination during coating and drying.[80] Yield stress, by contrast, is the threshold stress required to make a slurry flow, and below this threshold, the slurry behaves like an elastic solid.[90] An appropriate yield stress helps prevent particle settling during storage and maintains the shape of the coated film.[37,90]

Finally, extensional rheology, which describes a slurry's flow behaviours under elongational deformation, is increasingly recognised for its relevance in processes involving stretching or flow convergence, such as slot-die coating, inkjet printing, and the pinch-off dynamics during intermittent coating.[91,92] Extensional properties are sensitive to binder type and concentration, and cannot be modelled accurately form shear rheology measurements.[92]

It is worth emphasising again that these macroscopic rheological behaviours are direct manifestations of the underlying microstructures. The particle dispersion, homogeneity, binder distribution and the overall connectivity of the CBD collectively determine the slurry's response to external stress. Therefore, to achieve the desired macroscopic rheological profiles one needs to control the slurry's microstructures, and that in turn should be done through careful formulation and mixing configuration.

2.2 Slurry mixing configurations

It is a complex undertaking to meet the desirable microstructural and macroscopic rheological requirements consistently, across the laboratory and industrial scales. The final state of the slurry is not merely determined by its composition, but is critically dependent on the employed mixing processes, which involves a myriad of parameters, from heterogeneity in particle properties to the specific configurations of equipment.[93,94] Therefore, successful slurry formulation requires a process-sensitive approach, where mixing parameters are carefully adapted and controlled according to the intended material properties and slurry composition. This requires a comprehensive understanding on the influence of the main mixing configurations on the slurry microstructure and properties. Here we cover a few representative configuration parameters, but it is important to recognise that there are many more.

2.2.1 Equipment. The objective of mixing is to uniformly refine the agglomerates and aggregates, and assemble the particle components into a desired microstructure – without damaging the materials. There are broadly three categories of mixing devices: hydrodynamic shear mixing (*e.g.* planetary mixers, kneaders), mill (*e.g.* disc, roller, and ball mills) mixing and ultrasonic homogenisation, see Fig. 3(a). Hydrodynamic shear mixers relies on fluid motion to generate shear stress and break down clusters. Double planetary mixer, for example, can effectively achieve submicron cluster sizes.[95] Mill mixers, by contrast, rely on mechanical impact and shear in the milling process. They can achieve finer sizes than shear mixers,[96] but the high-intensity mechanical forces can damage the crystalline structures of the materials. Ultrasonic homogenisation for battery slurry is still an active research topic only in the early stages of industrial adoption. It uses high-power ultrasound (not to be confused with low-power ultrasound for inspection purposes) to generate localised shock waves through acoustic cavitation to aid mixing,[97] which is energy efficient and effective for concentrated slurries, but it poses risks of generating highly reactive free radicals and associated chemical degradations, particularly in aqueous slurries.[98]

2.2.2 Mixing ratios. The solid concentration and mass ratio of the components significantly impact slurry properties. Fig. 3(b) shows an example of shear viscosity *vs.* solid concentration. It reveals that there is an optimal window of solid concentration (the shaded region), which ensures the stability of the slurry structure against settling, while maintaining suitable rheological behaviours.[78] The mass ratio typically also has an optimal window. For instance, in the range of 0.4–1.0 wt%, polymer binder would enable sufficient adhesion on AM surfaces while promoting particle dispersion, whereas excessive polymers (>1.0 wt%) result in a solid-like gel structure ($G' > G''$) which reduces the slurry's processability, as demonstrated in Fig. 3(c).[89]

2.2.3 Component addition sequence. The sequence in which constituent materials are added during mixing can strongly affect slurry quality. For example, Lee *et al.*[100] demonstrated that for a $LiCoO_2$/CB/PVDF cathode slurry, adding the NMP solvent in multiple steps yielded better rheological properties and particle dispersion, resulting in superior cycling stability and rate performance, see Fig. 3(d). These findings were later corroborated by a mesoscale model.[101] Similarly, strong dependence on the mixing sequence was also found for anode slurries.[102]

2.2.4 Mixing duration and intensity. Typical mixing processes on a planetary mixer range from 2 to 6 hours, at speeds between 1000 and 4000 rpm. While higher speed and extended duration generally enhance particle dispersion, they could also lead to overmixing, which may end up disrupting the optimal microstructure of AM/CA clusters and damaging polymer binders, thus degrading battery performances.[103,104]

2.3 Summary and challenges for characterisation

The microstructures and macroscopic rheological properties of battery slurries are profoundly influenced by a broad range of mixing configuration parameters. Thus, the task of achieving ideal slurry properties becomes the optimisation of manufacturing parameters, which is a formidable task given that there

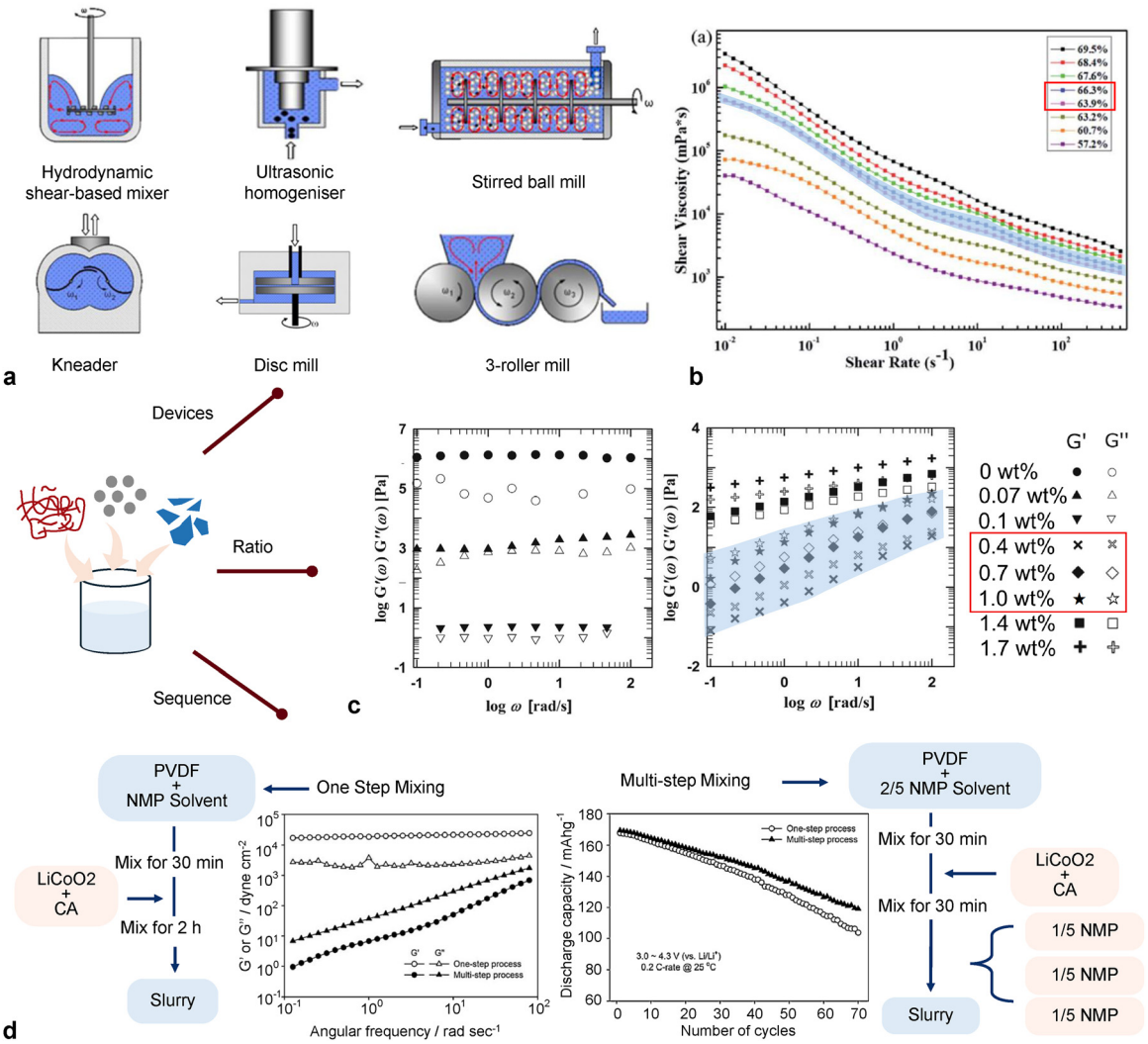

Fig. 3 Slurry mixing configurations and their effects on the slurry properties. (a) Schematics of several commonly used mixing devices. Reproduced with permission from ref. 99. Copyright 2011, Elsevier Ltd. (b) Slurry viscosity with various solid contents (57.2–69.5 wt%). The shaded region (63.9–66.3 wt%) indicates the optimal window of solid concentration which balances favourable rheological behaviours. Adapted from ref. 78. Copyright 2020, licensed under CC BY-NC 3.0, Royal Society of Chemistry. (c). The complex modulus of anode slurries composed of 50 wt% graphite and varying concentration of carboxymethyl cellulose (CMC). The shaded region (0.4–1.0 wt%) indicates the optimal binder ratio window where a balance between viscous and elastic responses is maintained ($G' \approx G''$), ensuring both particle dispersion and structural stability. Reproduced with permission from ref. 89. Copyright 2015, Elsevier Ltd. (d) The effect of different mixing sequences (one-setp mixing and multi-step mixing) on the rheological properties and battery capacity during cycling. Reproduced with permission from ref. 100. Copyright 2010, Elsevier Ltd.

are hundreds of interdependent variables in the optimisation space, and even subtle changes in the likes of particles formulation or mixing strategy can yield considerable differences in slurry property outcomes.

Fundamentally, the optimisation is an inverse problem, where we seek process inputs that would yield desirable property outputs. This could be helped by robust prediction of slurry behaviours. Theoretical or computational fluid dynamics tools have been employed to study flow patterns, turbulence and mixing efficiency,[105–107] but their current formulations are generally ill-suited for the polydisperse, non-Newtonian battery slurries, which are governed by particle–particle interactions (these will require rheological modelling, to be reviewed in Section 3). As a result, the optimisation largely falls back on an iterative process through experimental characterisation.

In this context, accurate and rapid characterisation of slurry properties becomes paramount, as it directly determines the efficiency in each iterative step of the multi-dimensional optimisation process. The next chapter is therefore dedicate to reviewing state-of-the-art characterisation and modelling techniques. However, as will be discussed, the majority of them are offline and thus inefficient.

3 State-of-the-art characterisation techniques

Various haracterisations are carried out at various stages of slurry mixing. Pre-mixing inspections primarily target incoming material quality and impurities detection (*e.g.* metal

particles). Techniques range from sieving to remove large aggregates in batch mixing, to applying magnetic fields for removing ferromagnetic contaminants. Advanced characterisations like inductively coupled plasma optical emission or various microscopies are sometimes employed to pinpoint the impurities at smaller scales.[108]

During and after mixing, slurries are evaluated to ensure conformance of specifications and to inform process optimisation. While limited real-time data on certain parameters can be obtained from inline sensors (*e.g.* bulk viscosity, from pressure dependence of rheological properties in a complex flow cell[109,110]) during mixing or transport, comprehensive characterisations of the slurry microstructures and macroscopic rheological properties rely most dominantly on offline techniques applied post-mixing. Complementary to direct experimental evaluations, modelling approaches are increasingly employed to elucidate the relationships between slurry microstructure, rheology and the mixing configurations, enabling more comprehensive and efficient optimisation strategies.

3.1 Direct experimental characterisations

3.1.1 Microstructures. As reviewed previously, it is crucial to characterise the key microstructural features of battey slurries such as PSD, homogeneity and dispersion, binder and CA networks, and surface chemistry, which are all dynamic and evolve throughout the mixing process. Table 1 summarise the existing techniques relevant to these characteristics, and Fig. 4 gives a graphic summary. It is important to recognise that these properties are not isolated but often interdependent; for instance, particle dispersion and aggregation behaviour both reflect the level of homogeneity.

To assess PSD, laser diffraction is commonly used in industry and research. It measures the angular intensity variations of scattered light as a laser beam passes through a dispersed particulate sample, since larger particles scatter light at smaller angles relative to the laser beam.[74] However, it struggles with highly opaque systems such as battery slurries and requires sample dilution, which would likely alter the microstructures. Dynamic light scattering (DLS) is another technique which offers finer resolution for nano-sized components. It measures particle motion in dispersion systems based on Brownian movement, where the energy transfer from particle–solvent collisions has a greater effect on smaller particles, resulting in higher speeds. DLS is limited to very dilute systems.[111] In practice, the Hegman gauge is a simple and rapid method to estimate the largest size of agglomerates or particles, though it lacks quantitative precision and is prone to user error.[112]

Advanced imaging techniques like SEM and cryo-SEM are commonly used to visualise slurry morphology, particle dispersion, and binder distribution. SEM is typically performed on a rapidly dried sample or on the finished electrode product,[113] thus it only offers indirect inference of the slurry state, and it struggles to resolve binders. Cryo-SEM preserves the slurry in a near-native state by rapidly freezing the liquid slurry, and can image binders more faithfully. Both techniques can achieve very high spatial resolutions down to 5–10 nanometres, capturing individual AM particles and CA networks.[33,89] Coupled with SEM, energy dispersive X-ray spectroscopy (EDS) enables precise, element-specific mapping across the sample, by detecting characteristic X-rays and visualising how different components are spatially distributed.[114] Raman spectroscopy is another technique used to evaluate slurry homogeneity, especially binder distribution,[115,116] given that most polymer binders contain Raman-active functional groups and exhibit strong vibrational modes. Quantitative dispersion information can be obtained through image-based processing of these results, *e.g.* by analysing contrast and pixel-intensity distributions in optical or SEM images.[117] Alternatively, analytical indices such as the Carbon Black Dispersion Index (DI_{CB}) can be derived from laser diffraction data to decouple bimodal particle size information and quantify the dispersion state.[118]

Understanding surface chemistry and interfacial properties is also important. Zeta potential measurements provide insights into the electrostatic repulsion or attraction between components, which help infer binder adsorption affinity and stabilisation mechanisms.[119] Additionally, Fourier transform infrared spectroscopy (FTIR) is another technique frequently used to evaluate probe particle-binder interactions and polymer structure formation, by detecting characteristic spectral shifts of functional groups present in binder materials.[120] Complementary to these, tensiometer technique (*e.g.* Wilhelmy plate or sessile drop method) measures surface or interfacial tension from the wetting force or droplet profile, providing insights on slurry wetting, coating uniformity, and formulation-dependent capillary effects.[121]

Furthermore, given the acknowledged link between slurry microstructure and electrode morphology, some characterisations are performed on the finished electrodes themselves. Techniques such as X-ray computed tomography (CT),[122] destructive focused ion beam scanning electron microscopy (FIB-SEM)[123] provide 3D morphological information, including essential properties like porosity and tortuosity. However, since there are multiple intermediate steps – coating, drying, and calendaring – that can alter final electrode properties, these evaluations are best treated as complementary for slurry optimisation rather than direct characterisation tools for the liquid slurries themselves.

3.1.2 Rheology. The macroscopic rheological properties are normally evaluated in a practical sense, to deliver insights on the processability and structural integrity of the slurries, and directly inform the mixing process optimisation as well as the subsequent coating and drying steps, as summarised in Table 2 and Fig. 5. Prior to rheological testing, bulk density and solid content are often determined using pycnometry or vibrating-tube densimeters, to evaluate the slurry's mass-to-volume ratio and solids loading.

Shear viscosity measurements are typically performed using rotational rheometers, which measure the torque required to rotate a specific geometry (parallel plates, cone-and-plate, or concentric cylinders) with a small amount of slurry sample placed in the gap. Simpler rotational viscometers (*e.g.* the Brookfield type with an immersed spindle) are also often utilised (in some cases inline[26,140]) for basic quality control. Alternatively,

Table 1 Characterisation techniques for slurry microstructure

Specification	Techniques	Working principles	Spatial resolution	Capabilities & limitations
Particle size PSDs aggregates agglomerates	Laser diffraction[124]	Measure the angular variation in intensity of light scattered by a particulate sample	✗	✓ PSD distribution ✓ Sample volume in milliliters ✗ Require sample dilution ✗ Localised result
	Dynamic light scattering[125]	Measures fluctuations in scattered light intensity caused by Brownian motion of particles	✗	✓ Resolution to nanoscale ✓ Sample volume in microliters ✗ Require sample dilution ✗ Localised result
	Hegman gauge[32]	A stainless-steel block containing grooves with graded slopes	✗	✓ Different sizes available ✗ Qualitative not quantitative ✗ Prone to human error ✗ Small inspection scale
Homogeneity (particle dispersion, binder distribution)	SEM[126]	Use an electron beam to image samples with a resolution down to the nanometer scale	nm	✓ Elemental-wise spatial distribution ✓ Resolution to microns ✗ Sample preparation ✗ Small inspection scale
	Cryo-SEM[89,127,128]	Rapid freezing of liquid sample for SEM	nm	✓ Near-native slurry state ✗ Additional sample preparation ✗ Localised results
	EDS[129,130]	Measure the energy and intensity of the X-rays emitted by a sample	μm	✓ Elemental-wise spatial distribution ✗ Complex sample preparation ✗ Small probing depth ✗ Low sensitivity to light elements
	Raman spectroscopy[115,131]	Measure interaction of light with the chemical bonds of a substance	1 μm in depth	✓ Binder distribution ✓ Binder-AM interactions ✗ Limited probing area and depth ✗ Require strong Raman-active modes
	Image-based dispersion analysis[117]	Analyse contrast and pixel-intensity distributions in optical/SEM images to yield a dispersion index	μm	✓ Quantitative information ✗ Sensitive to imaging quality/thresholding ✗ Indirect measure (not particle size)
	Analytical-based dispersion index (DI_{CB})[118]	Decouples bimodal PSD information from laser diffraction data to quantify CB dispersion *via* mathematical analysis	✗	✓ Quantitative CB information ✓ Tracks de-agglomeration progress ✗ Sample preparation ✗ Require pre-analytical results
Surface chemistry	Zeta potential[94,126]	Measure the electrical potential at the slipping plane of particles in a suspension	✗	✓ Provide electrostatic information ✓ Infer Stability mechanisms ✗ Lack spatial details ✗ Sensitive to condition (*i.e.* pH)
	FTIR[120,132]	Measures characteristic spectral absorptions of functional groups	~10 μm	✓ Identify specific functional groups ✓ Monitor binder interactions ✗ No spatial distribution ✗ Sensitive to condition (*i.e.* moisture)
	Tensiometer[121]	Measure surface or interfacial tension from wetting force or droplet profile	✗	✓ Interfacial tension and wettability ✓1 Useful for coating ✗ No spatial mapping ✗ Sensitive to evaporation and temperature
Electrode morphology	X-CT[133–135]	Reconstruct 3D internal structures by measuring X-ray attenuation through a sample	~1–10 μm	✓ 3D morphology – porosity and tortuosity ✗ Indirect to slurry evaluation ✗ Long scanning time ✗ High equipment costs
	FIB-SEM[136,137]	Combine ion beam milling with electron imaging to visualize high-resolution cross-sectional microstructures	nm	✓ High-resolution cross-sectional imaging ✗ Indirect to slurry evaluation ✗ Destructive – sample ablation required ✗ Limited field of view

slurry viscosity can be inferred using pressure difference measurements over a known geometry, such in the transportation pipes from the mixer to coater, where the pressure drop reflects the flow resistance and the rheological behaviours of the slurry.[32,38] These tests typically cover a broad range of shear rates, *e.g.* 0.1 to 1000 s^{-1},[80,141] which are still limited compared to real manufacturing processes, especially coating, given that shear rates can range from 500 to 10 000 s^{-1} between research drawdown and industrial reel-to-reel coaters.[80] The experimental results are typically fitted and extrapolated to give the responses in the wider shear rate ranges.[141]

Thixotropy is usually also evaluated using rotational rheometers. Common methods include: step-shear rate tests (*e.g.* the three-interval Thixotropy Test, 3iTT[142]), where the sample is subjected to periods of contrasting shear rates in succession, allowing the time-dependent recovery of viscosity or structure

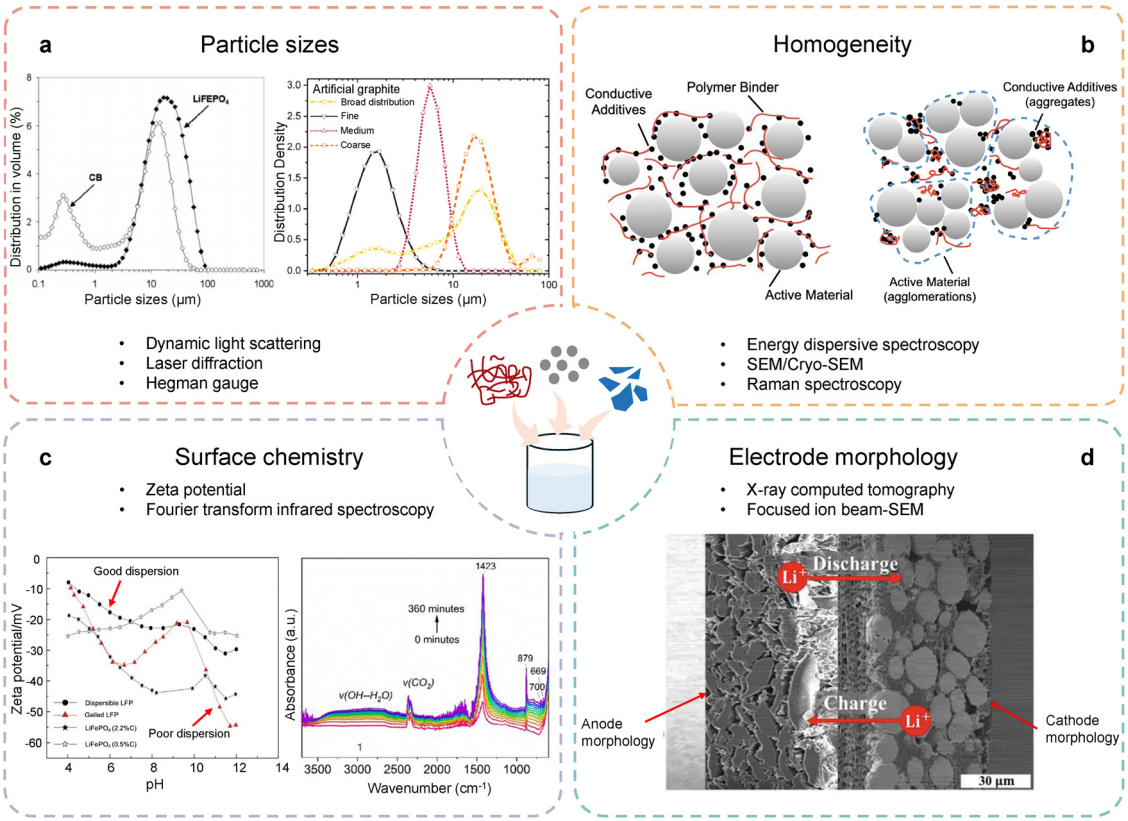

Fig. 4 Schematic summary of microstructural characterisation techniques for battery slurry systems. (a) Particle sizes and PSDs: representative examples of typical PSD results with bimodal or multimodal patterns obtained from laser diffraction or dynamic light scattering techniques. Left: Reproduced with permission from ref. 72. Copyright 2008, Electrochemical Society. Right: Reproduced from ref. 138. Copyright 2020, licensed under CC BY 4.0, Wiley-VCH (Chemistry Europe). (b) Slurry homogeneity: comparison between good and bad dispersions; (c) surface chemistry: representative data from zeta-potential and FTIR measurements, which probe particle–binder interactions and surface functional groups. Left: Reproduced with permission from ref. 94. Copyright 2016, Elsevier Ltd. Right: Reproduced from ref. 120. Copyright 2022, licensed under CC BY 4.0, Elsevier Ltd. (d) Electrode morphology: cross-section imaging obtained from X-ray tomography. Reproduced from ref. 139. Copyright 2018, licensed under CC BY 4.0, Electrochemical Society.

to be monitored; and hysteresis loop tests,[88] by observing the response hysteresis when the shear rate is continuously ramped up and then immediately ramped down.

Oscillatory rheological tests are commonly use to probe the viscoelasticity of battery slurries, by applying a small sinusoidal shear strain or stress and measuring the response. Small amplitude oscillatory shear (SAOS) is the most commonly reported method, which is performed within the linear viscoelastic region so that the responses are proportional to the applied deformation. SAOS gives the frequency-dependent energy storage modulus (G') and the energy dissipation loss modulus (G'').[143] The magnitudes and frequency dependence of these moduli provide a means to infer the internal network microstructures,[78] and to optimise formulation (*e.g.* by identifying the maximum solid concentration the slurry can accommodate for optimal flow[80]). In contrast, large amplitude oscillatory shear (LAOS) operates beyond the linear viscoelastic region, inducing non-sinusoidal responses and higher harmonics, which can infer yielding and structural breakdown kinetics.[144]

As for yield stress, several test methods can be performed on rotational rheometers. Flow curve data of shear stress as a function of shear rate can be extrapolated to zero shear rate using Herschel–Bulkley or Bingham models.[80,129] Alternatively, a stress ramp can be applied and the yield stress can be identified as the stress value at which significant flow initiates, often indicated by a sharp increase in strain or strain rate.[145,146] Oscillatory amplitude sweeps can also indicate yielding stress, where the storage modulus significantly deviates from linearity or drops sharply, indicating network breakdown.[90]

The characterisation of extensional rheology presents significant challenges. While techniques such as stop-flow dripping-onto-substrate/capillary break-up rheometry (SF-DoS/CaBER)[147] can obtain reliable results,[92] they require complex experimental setup and high precision to capture rapid filament thinning and pinch-off dynamics,[148] which are particularly challenging for the highly viscous battery slurries. Reynolds *et al.* developed a low-cost, miniaturised extensional rheometer[91] that overcomes the difficulties to enable rapid, small-volume measurements, and reveals extensional behaviours not captured by shear tests, further underscoring the importance for direct extensional measurements in slurry optimisation.

Table 2 Characterisation techniques for slurry rheological properties

Specifications	Testing approach	Working principles	Capabilities & limitations
Shear viscosity	Rotational rheometry[36]	Measure torque as a function of angular velocity	✓ Steady shear flow response ✗ Offline testing ✗ Limited maximum shear rate
Thixotropy	Rotational rheometry[78,149]	Measure viscosity in a time-dependent controlled-shear-rate manner	✓ Assess shear recovery behaviour ✗ Offline testing ✗ Long testing time
Viscoelasticity	Small amplitude oscillation shear (SAOS)[36,150]	Apply small oscillatory strain and measure stress response	✓ Slurry complex behaviours ✓ Useful for process optimisation ✗ Sensitive to local heterogeneity ✗ Offline testing
Yield stress	Large amplitude oscillation shear (LAOS)[145,146]	Apply large oscillatory strain and identify the G' drop or G', G'' crossover	✓ Onset of non-linearity ✓ Qualitative yielding behaviours ✗ Data interpretation complexity ✗ Offline testing
	Rotational rheometry with model fitting[151]	Shear rate sweep and fit stress-shear rate curve to extract σ_0 (yield stress at zero shear rate)	✓ Quantitative yield stress ✗ Additional model fitting ✗ May suffer from wall slip at low shear
	Rotational rheometry with stress ramp test[145,146]	Apply stress ramp and monitor the point where flow begins	✓ Onset of yielding ✓ Independent of model assumption ✗ Sensitive to surroundings ✗ Offline testing
Extensional rheology	Capillary thinning rheometry[92]	Monitor filament thinning dynamics during capillary breakup	✓ Direct relevance to coating ✓ Sensitive to different compositions ✗ Difficult to pinpoint the breakup point ✗ No standardised machine ✗ Low data repeatability
	Filament stretching rheometry[91]	Stretch a filament between plates and measure extensional viscosity	✓ Direct relevance to coating ✓ Sensitive to different compositions ✗ Sensitive to boundary conditions ✗ Limited accessibility

3.2 From microstructures to rheology: predictive modelling

While the direct experimental characterisations provides essential data on specific properties of the slurries, they typically cover limited test conditions and do not fully capture the dynamic interplay between structure and flow behaviour under all relevant processing conditions. Predictive modelling approaches are increasingly employed to bridge the gap and complement the experimental techniques. The primary goal of such models is to estimate the macroscopic rheological responses, relying not on exhaustive physical testing but on the microstructure information and fundamental laws.

For example, a widely used approach to quickly estimate rheological behaviours is through empirical or semi-empirical suspension models, which assume homogeneously dispersed, rigid particles. Among the most widely used are the Herschel–Bulkley equation[36,37,152] to describe the shear stress with respect to the non-Newtonian flow behaviours, and the Krieger–Dougherty[79,80,153] (or Quemada[154]) model to relate viscosity to particle volume fraction and maximum packing. In contrast, recent developments focus on capturing more comprehensive and accurate microstructure specifications through micro-rheological modelling or multi-scale simulations, while data-driven models provide alternative avenues to establish correlations.

Physics-based micro-rheological modelling seeks to predict bulk rheology such as viscosity flow curves, by explicitly incorporating fundamental physical interactions within the slurry. Two types of interactions are primarily considered: inter-particle colloidal interactions (*e.g.* van der Waals attraction, steric hindrance, and electrostatic repulsion) and hydrodynamic interactions (*e.g.* shear-induced drag and Brownian motion). The former are particularly significant for smaller particles, such as carbon black in a slurry system, while the later for large particles and aggregates. For example, Ma *et al.*[87] developed a microrheological model for anode slurries, treating viscosity as the sum of hydrodynamic interactions (captured using Krieger's formula) and structural contributions from colloidal forces forming fractal aggregates and transient networks[157](Fig. 6(a)). The model showed good agreement with experimental data across a range of slurry compositions and carbon black contents.

Multi-scale simulation models offer a bottom-up computational approach to predict slurry behaviour across different length and time scales. Coarse-grained molecular dynamics (CGMD) and discrete element method (DEM) are two commonly used methods to simulate slurry structures, by explicitly accounting for attractive and repulsive fields between the particles, enabling the particle movements during dynamic processes to be tracked.[155] Duquesnoy *et al.*[156] developed a mechanistic CGMD model that incorporated realistic slurry composition, including the mass AM-to-CBD ratio and the

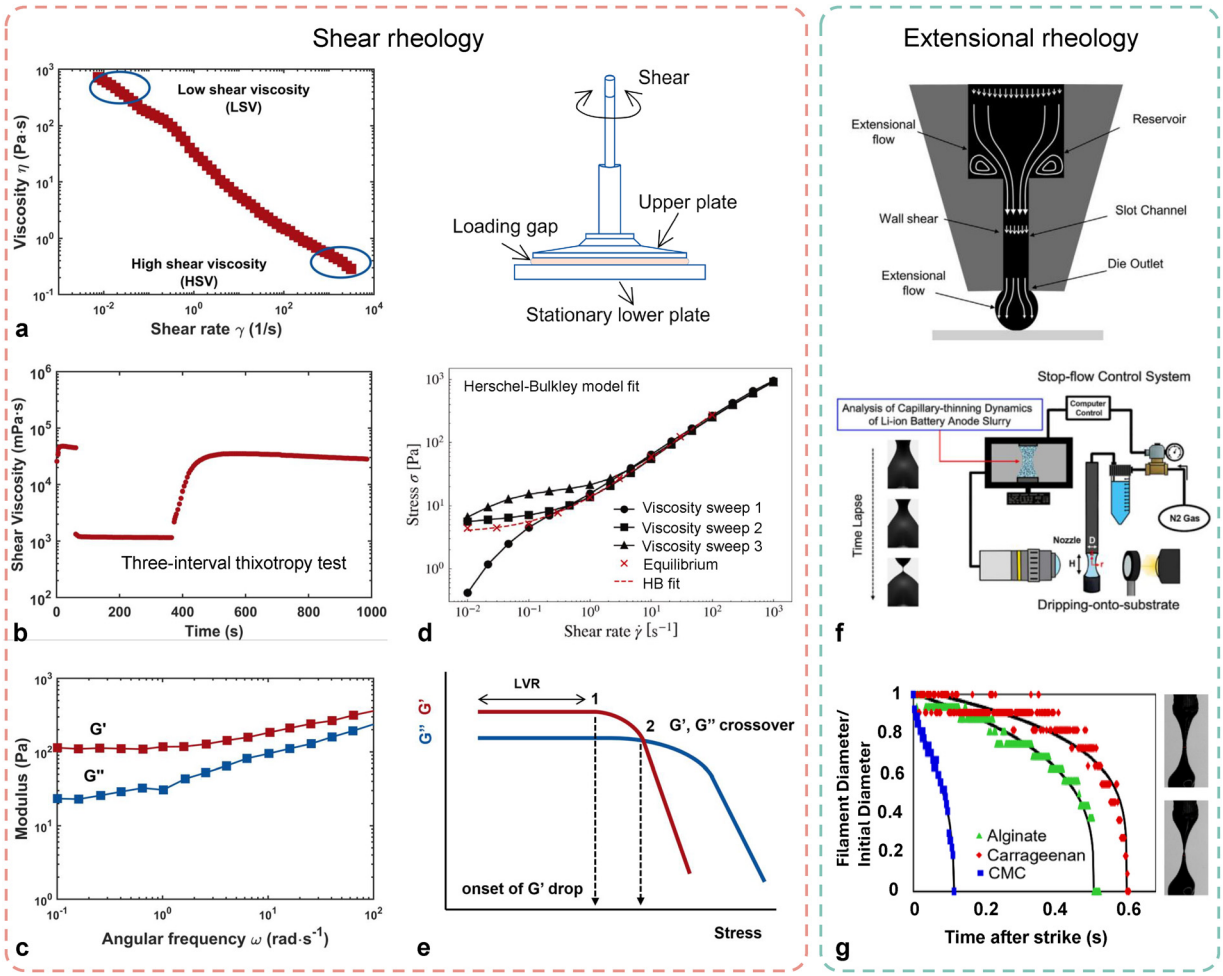

Fig. 5 Rheological characterisation of battery slurries, including (a) viscosity flow curve. Data extracted from ref. 71 and replotted by the authors. (b) Thixotropic property. Data extracted from ref. 78 and replotted by the authors. (c) Viscoelasticity. Data extracted from ref. 71 and replotted by the authors. (d) Yield stress obtained through model fitting. Reproduced with permission from ref. 86. Copyright 2024, Elsevier Ltd. (e) Yield stress obtained from complex modulus. Data extracted from ref. 145 and replotted by the authors. (f) Extensional rheology obtained from capillary thinning setup. Reproduced with permission from ref. 92. Copyright 2024, Elsevier Ltd. (g) Extensional rheology by filament stretching. Reproduced with permission from ref. 91. Copyright 2022, Elsevier Ltd.

PSD, as displayed in Fig. 6(b). They then applied non-equilibrium molecular dynamics (NEMD) to simulate the evolution of slurry microstructure under defined shear and computed the corresponding shear viscosity – see Fig. 6(c). Such mechanistic framework provide a powerful platform for linking microstructure to rheology, and can potentially be extended, *e.g.* using DEM, to study thedrying and calendaring processes.[158] However, full multi-scale simulations are computationally demanding, their outputs can be used to train light-weight surrogate models.

Data-driven models provide a powerful alternative to physics-first approaches, aiming to correlate slurry microstructures or formulation parameters with rheological properties, without resolving all underlying physics explicitly. They leverage the extensive availability of experimental data and rapid advancements in machine learning (ML). A wide range of ML models, including neural networks,[159,160] random forests,[161,162] and Gaussian processes,[163,164] have been explored for battery manufacturing and characterisation, as summarised comprehensively in ref. 165. Applying explainable ML techniques on battery slurries, Reynolds *et al.*[166] demonstrated that even small experimental datasets (<30 formulations) could be used to investigate the effects of AM, CA, and binder concentrations on viscosity and electrode performance. Liu *et al.*[167] further showed that Gaussian regression enables not only accurate prediction of electrode mass load, but also directly quantification of the relative importance of mixing and coating parameters. Additionally, in an effort to reduce reliance on large experimental datasets, Duquesnoy *et al.*[168] developed a hybrid modelling framework, combining CGMD and NEMD simulations with surrogate ML models to accelerate the inverse optimisation of slurries under multiple constraints, achieving over tenfold reduction in computation time without sacrificing predictive accuracy. Together, these studies illustrate how data-driven approaches can complement physical modelling and practical process control, and support the predictive optimisation of battery slurries and smarter manufacturing.

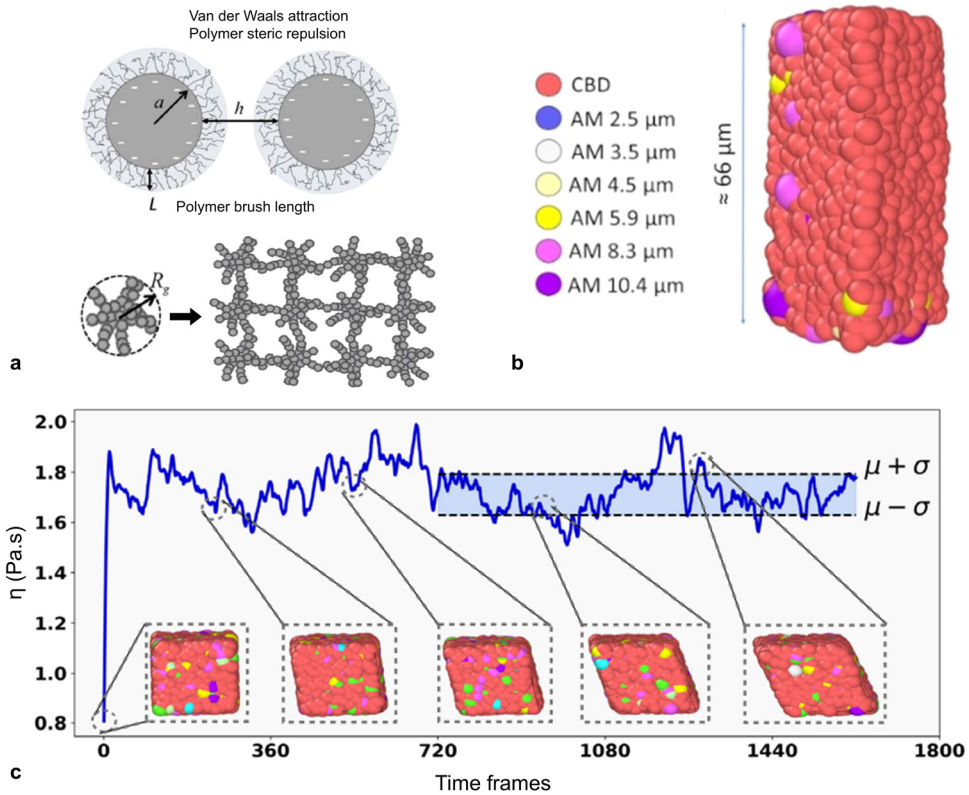

Fig. 6 (a) Schematics of polymer-coated carbon black particles and interparticle colloidal interactions, and primary carbon black particles assembled into secondary aggregates connected into networks. Reproduced with permission from ref. 87. Copyright 2019, Elsevier Ltd. (b) Schematics of a simulated slurry, where CBD and PSD of AM particles are considered and randomly placed. Reproduced from ref. 155. Copyright 2020, licensed under CC BY 4.0, Wiley-VCH (Chemistry Europe). (c) The slurry microstructure evolution and associated viscosity (η) during NEMD simulation were handled to assess the slurry viscosity at a given shear rate (γ). The last 1000 viscosity values from a single simulation are used as a vector to calculate an average value (μ) and a standard deviation (σ). Reproduced from ref. 156. Copyright 2022, licensed under CC BY 4.0, Springer Nature.

3.3 Prospects for slurry characterisation

Whereas a broad array of experimental techniques and modelling approaches aim at understanding battery slurry properties, the fact that most are offline remains a significant challenge. This often necessitates time-consuming sample preparation and provides only intermittent snapshots of slurry quality, breaking down the feedback loop to the parameter optimisation process.

Therefore, future characterisation strategies should ideally integrate inline, real-time monitoring with predictive modelling. Inline sensors could provide agile, continuous data on key slurry attributes, while robust models, informed by this real-time data, could predict overall behaviour and reduce the need for exhaustive offline characterisation of every property.

4 Ultrasonic characterisation of slurries

Low-power ultrasound presents a compelling solution to the inline monitoring requirements highlighted above. As mentioned, it has a long history of successful applications in the mining, food, and pharmaceutical industries.[50,52–54] Recent reviews[169,170] have emphasised the growing relevance of ultrasonic methods for the analyses of LIB life cycles, which reinforce ultrasound's credentials for characterising material properties even at the slurry stage.

A thorough understanding of the state-of-the-art in ultrasonics is crucial to contextualise the proposed inline characterisations. This section will therefore delve into the two aspects of ultrasonic analysis: the characterisation of slurry microstructures and the measurement of macroscopic rheology. For each aspect, we will first detail the established theoretical principles and experimental methods, and then immediately highlight the critical research gaps were these techniques to be applied to the uniquely complex battery slurries. These sequential analyses will cumulatively build a comprehensive case for the new, integrated framework presented in Section 5.

4.1 Fundamentals of ultrasound

4.1.1 Ultrasonic wave modes. Ultrasound refers to high-frequency (>20 kHz) sound waves, typically in the megahertz (MHz) range for materials characterisation. They are classified as either compressional (longitudinal) waves, where the particle motion is parallel to the wave propagation direction, or shear waves, where the two directions are perpendicular to each other, as shown in Fig. 7(a) and (b). Compressional waves can travel through both solids and fluids, while shear waves primarily

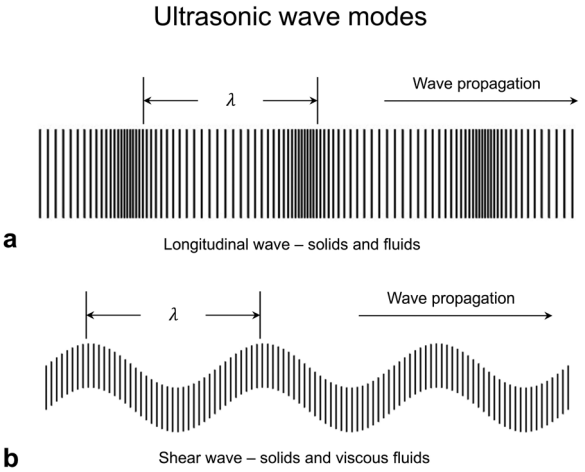

Fig. 7 Ultrasound wave modes classification: (a) compressional (longitudinal) wave, whose particle motion is parallel to the wave propagation direction and (b) shear wave, whose particle motion is perpendicular to the wave propagation.

propagate in solids and can only penetrate into viscous fluids in micron-scale depths (depending on the fluid's viscosity[171]).

Ultrasound interacts with the constituents of the slurry, through mechanisms to be discussed later in Section 4.2, leading to detectable behaviours such as changes in wave speed and attenuation (reduction in wave amplitude per unit distance), and backscattering (noise-like signals scattered back to the emitting transducer by suspended particles). The former two properties can be mathematically expressed in the harmonic wave equation, see Appendix A. The interactions are dependent on the ultrasonic wavelengths (and frequency) and the particle sizes in the slurry, and the characterisation of slurry properties relies on precise experimental measurements of the detectable changes, especially how they vary with frequency in a broad spectrum.[40,172]

4.1.2 Experimental measurement setups. A typical ultrasonic measurement setup is illustrated in Fig. 8(a). An ultrasonic pulser/receiver sends electrical pulses at high repetition rates (hundreds of pulses per second) to the piezoelectric transducer, which converts the pulses to propagating ultrasonic waves into the sample. The receiving transducer converts incoming waves into electrical signals for visualisation or storage. The propagation time through a mm-scale sample is in μs, enabling real-time experiments.

Wave speed and attenuation in slurries are often measured together, using the configurations shown in Fig. 8(b) and (c). In through-transmission, the transmitting and receiving transducers are aligned coaxially on the opposite sides of the sample; whereas in pulse-echo, a single transducer both transmits and receives the ultrasonic signal from an acoustic reflector. The acquired signals are then analysed in the frequency domain to extract wave characteristics, due to the dispersive nature of battery slurries (*i.e.* wave speed varies with frequency). Attenuation is typically determined *via* ultrasonic attenuation spectroscopy (UAS),[39,173,174] by comparing the frequency-domain amplitude spectra from the slurry and a reference medium (*e.g.* deionised water), as described mathematically in Appendix B. These experimental setups and analyses (particularly UAS) are central to ultrasonic characterisation of slurry microstructures.

A common setup for measuring backscattering is shown in Fig. 8(d),[175] which analyses the noise-like signals scattered back by suspended particles. It commonly incorporates a delay line on the transducer, to ensure that signal detection occurs in the far field and that the backscattered signals are temporally resolved from the initial transmission. Backscattering data are usually interpreted statistically,[176] with the maximum amplitude (b_{max}) and time-dependent decay (β) sensitive to particle size and concentration. However, the complexity introduced by multiple scattering effects poses challenges to accurate data interpretation.[175]

In addition to these bulk wave setups, guided waves are also widely employed, especially for measuring viscosity and viscoelasticity (to be discussed in Section 4.3), as illustrated in Fig. 8(e). Guided waves are acoustic waves that propagate along, and confined by, geometric features known as waveguides, such as plates, pipes, or thin rods – a classic example is the string in a tin-can phone. They are particularly sensitive to the slurry properties in close proximity to the boundaries, and are mainly used to characterise macroscopic rheology.

4.2 Ultrasonic characterisation of slurry microstructures

The microstructure of a slurry (*e.g.* PSD or concentration) fundamentally governs most of its macroscopic properties and behaviours (as established in Section 2), so they have thus been a central focus for the ultrasonic characterisation of colloidal suspensions in literature. Fundamentally, this is enabled by the sensitivity of ultrasound to the nature of scatters and solid concentration when working at long wavelength (*i.e.* wavelength $\gg$ suspended particle size). Examining how this characterisation works is the objective of this section, and also core to the inline monitoring of battery slurries proposed in this paper. Note that this field has a huge volume of work, this section only provides a snippet of research relevant to high-loading slurries; refer to *e.g.* ref. 40 for a more comprehensive review.

4.2.1 Wave-slurry interactions: phenomenological mechanisms. Ultrasonic waves propagating through a slurry interact with the suspended solid particles *via* several physical mechanisms, which originate from the different material properties (*e.g.* density, compressibility, thermal conductivity) between the particles and continuous phase (fluid), and can be summarised to five primary mechanisms,[40] as illustrated in Fig. 9. Their relevances to battery slurries are discussed below.

Material substitution (Fig. 9(a)) is the simplest phenomenon, referring to the effects on the propagating wave caused by the suspended particles replacing the continuous fluid medium. This is a dominant contributor to attenuation and velocity changes (which can be approximated by a weighted average of the two phases, after accounting for wave diffraction effects *etc.*) in concentrated battery slurries with dense solid particles (*e.g.* NMC and graphite).

Density contrast (Fig. 9(b)) between the solid particles and fluid causes inertia differences, resulting in the particles resisting

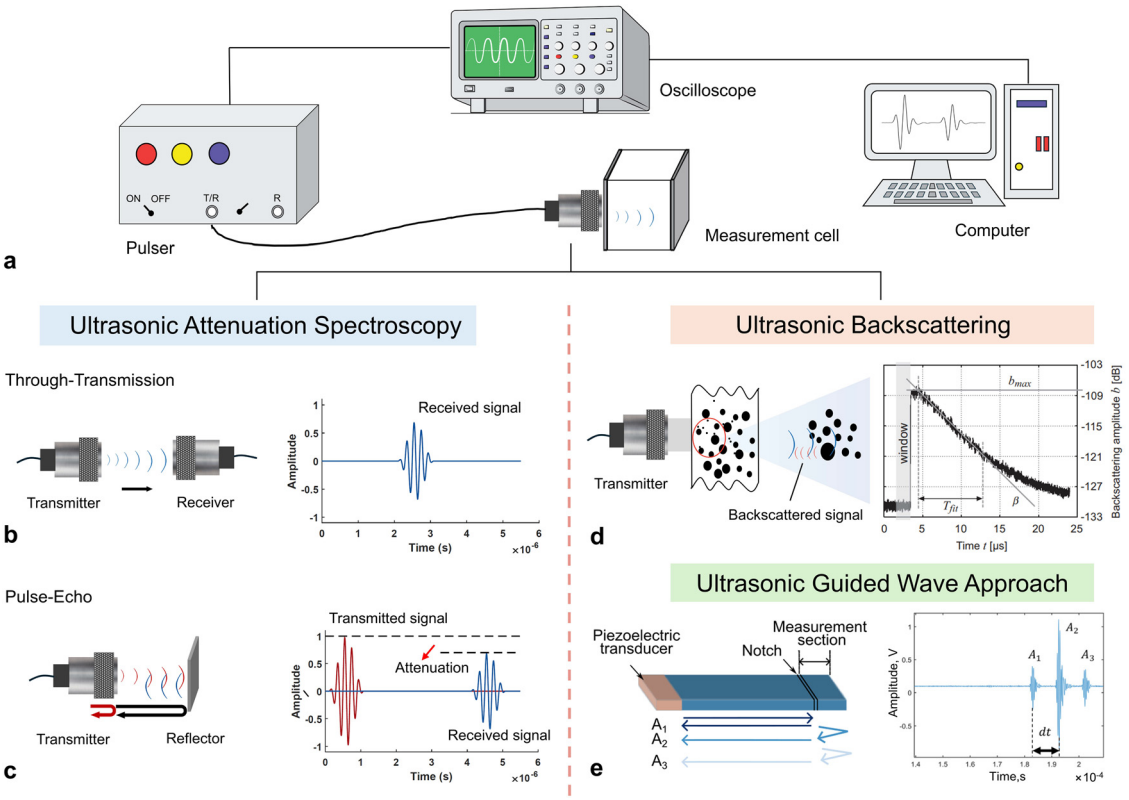

Fig. 8 Experimental ultrasonic measurement configurations. (a) Electronical devices in a typical experimental setup; (b) the ultrasonic attenuation spectroscopy with transducer arranged in through-transmission and (c) pulse-echo manners; (d) ultrasonic backscattering measurement. The left plot shows the typical setup and the right plot (reproduced from ref. 175 with permission) a typical backscattered signal time trace; (e) ultrasonic guided wave approach for macroscopic property measurement. The left plot shows a dip-stick setup and the right the typical time trace to evaluate viscosity-induced attenuation (reproduced from ref. 177 licensed under CC BY-NC 4.0).

acceleration and the fluid exerting a viscous drag on them – this is known as visco-inertial effects – during the pressure oscillations of the wave. These lead to scattering, partial reflection, and attenuation of the propagating ultrasound. In battery slurries, this is highly relevant given the significant density contrast between the phases.

Multipole resonances (Fig. 9(c)) occurs when the acoustic wavelength becomes comparable to the particle size, causing the particle to undergo resonant oscillations and act as a strong multipole radiator. This leads to sharp attenuation peaks at resonance frequencies. While well-mixed battery slurries have typically >50 MHz particle resonances (assuming 1–10 μm size), aggregates or agglomerates (10–100 μm) in the intermediate states can exhibit resonances within the commonly used ultrasonic range (<20 MHz). This mechanism could be exploited for monitoring clusters during mixing.

Compressibility and thermal contrasts (Fig. 9(d) and (e)). Compressibility contrast stems from differences in bulk modulus between the particles and fluid, resulting in deformations to different extents under acoustic pressure, and a monopole radiation pattern from the particles. Thermal contrast can induce attenuation as the local pressure fluctuations caused by ultrasound result in cyclic temperature changes in both particles and fluid, leading to thermal diffusion and energy loss. However, in battery slurries, both effects are generally minor, due to the low compressibility, μm sizes and high thermal conductivity of most battery materials.

It is important to highlight that although the nominal solid concentrations in battery slurries – typically 50–60 wt% ($\simeq$20–25 vol%) for NMC cathode and 40–60 wt% ($\simeq$25–40 vol%) for graphite anode[80] – are not exceptionally high, these slurries exhibit pronounced, highly viscous non-Newtonian behaviours primarily caused by the polymeric binders in the continuous phase, which form entangled networks and adsorb onto particle surfaces, dramatically increasing effective volume fraction and inter-particle interactions. As such, they are substantially different from simple suspensions which the classic research (reviewed in the next subsection) are based upon, but instead behave like a viscoelastic composite with both solid- and fluid-like characteristics.

4.2.2 The forward modelling of ultrasonic behaviours. Generally speaking, theoretical models incorporate the physical mechanisms (multiple mechanisms often coexist in dense slurries and are handled simultaneously) to solve a forward problem: predicting the ultrasonic behaviours (wave speed, attenuation and backscattering) based on known slurry characteristics (*e.g.* PSD, concentration, and constituent material properties). A primary focus is the frequency-dependent wave

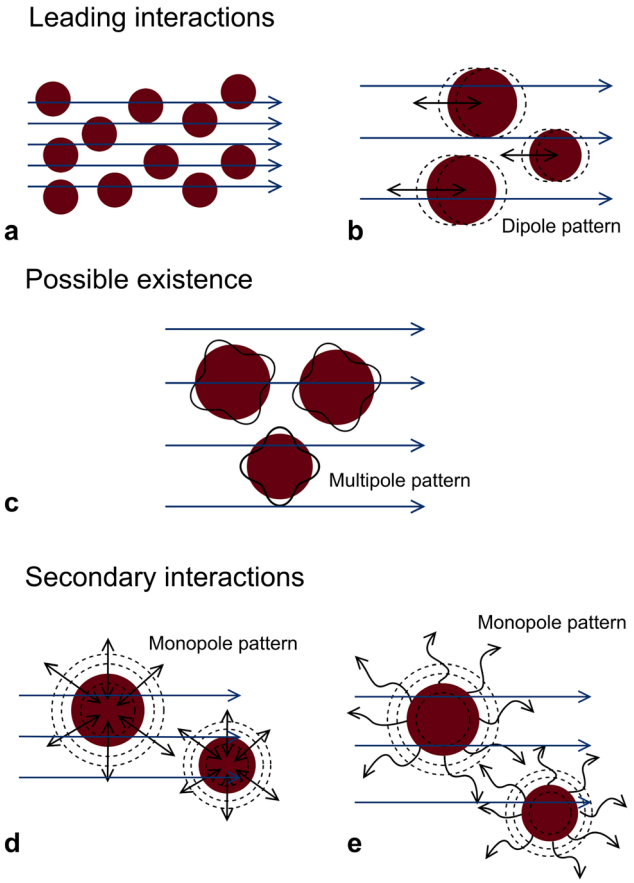

Fig. 9 Leading interaction mechanisms between ultrasonic waves and a suspended particle in a concentrated slurry.[40] (a) Material substitution; (b) density contrast; (c) multipole particle resonance (strong when incident wave length matches resonance). Secondary mechanisms: (d) compressibility contrast; (e) thermal contrast.

attenuation coefficient $\alpha(f)$, which is sensitive to slurry microstructures and can arise from absorption (conversion of wave energy to heat), scattering (redirection of wave energy) and viscoelastic loss in the case of battery slurries. The classic models typically start with the wave scattering/diffraction for a single particle, followed by the assembly of these effects in a volume of distributed scatterers. The final form is an explicit expression of the total attenuation $\alpha(f)$ or wave speed, which allow convenient validation against experiments.

In systems where the particles are spherical or can be approximated as such, the seminal ECAH model (Epstein & Carhart[44] and Allegra & Hawley[45]) provides a rigorous way to calculate the colloidal scattering coefficients, as detailed in Appendix C. It explicitly include a non-propagating thermal waves in addition to compressional and shear waves, and the scattering coefficients for all wave modes are determined by enforcing mechanical and thermal continuity at the interface through a transition matrix. In practice, the compressional wave coefficient is of primary interest, since it is easily detectable by a transducer. In the assembly step, the original ECAH model adopted the simplest single-scattering assumption, calculating the total response as a linear summation of scattered waves by individual particles,[44,45,178] which was later shown to be inadequate to capture the complex interactions in concentrated colloidal systems.[179,180] Nevertheless, it remains a foundational model upon which many subsequent models are based.

As the solid concentration increase, multiple scattering, where scattered waves from one particle interact with its neighbours before reaching the detector, starts to dominate. This is accounted for by multiple scattering models such as the classic Llyod/Berry formulation[181] and others based on ensemble averaging (*e.g.* Fikioris and Waterman[182]), which extend ECAH to moderate concentrations ($\sim$20 vol%). However, their accuracy diminishes as the concentration further increases, due to the neglected direct particle–particle and shear wave interactions.[183–185] One advanced approach suitable for $>$30 vol% solid loading is the multimode multiple scattering model, developed by Luppé,[186] Pinfield and Forrester,[187,188] Pinfield and Valier-Brasier[189,190] and other workers, which explicitly accounts for shear waves propagating through the viscous fluid in the narrow gaps between adjacent particles. It significantly alleviates the limitation of the ECAH/LB model and gives accurate predictions at up to 35 vol% concentration.[187,189,190]

Another strategy for slurries with high solid loading is the core–shell approach, which originated from physical shell-coated structures (see *e.g.* ref. 191 and 192). Anson and Chivers[193] adapted it to the ECAH framework for a spherical particle surrounded by a concentric shell of the continuous phase. Boundary conditions are enforced at both fluid–shell and shell–core interfaces to account for near-field hydrodynamics. Later, Hipp *et al.*[194] applied the core–shell approach to derive effective propagation properties for a suspension of particles, which was later validated experimentally[195] for silica slurries up to $\sim$40 wt% (25 vol%). This model appears relevant to the binder-adsorbed AM particles in battery slurries. However, it has limited capability to accommodate polydisperse (*i.e.* different-sized) particles; its physical basis may not be as strong as the multiple scattering theories, and its applicable concentration ranges have also been superseded by the latter.

All models reviewed above are based upon ECAH, but alternative, independent ones also exist. Effective medium theories (EMTs)[184,196] treat the slurry not as a collection of discrete scatterers but a composite continuum. The wave propagation is described through homogenised properties, such as density, compressibility, and viscosity, according to those of the constituent phases. Coupled-phase models (CPMs)[197–199] model the dynamic interactions between particle and fluid phases through viscous drag and stress transfer mechanisms, and were shown to approximate the significantly more complicated core–shell model well, when the acoustic radius is small.[200] Recently, Monte-Carlo methods (MCMs) have emerged as a computational tool for modelling ultrasonic attenuation in complex slurries.[201–203] They do so by tracking probabilistic paths of wave packets through the particle field, naturally handling complex particle geometries, polydispersity, and random spatial distributions. The incorporation of particle–particle interactions and effective medium corrections enables accurate predictions up to 35–40 vol%.[202]

While much of the theoretical work has focused on attenuation, the same fundamental mechanisms also govern ultrasonic backscattering.[175,204] Models have been adapted to predict the

statistical characteristics of the signal scattered back towards the transmitter, which is particularly useful as it requires access from only one side of the sample. Ultimately, these forward models, which predict acoustic behaviours from known slurry characteristics, provide the foundation for solving the inverse problem: to determine unknown slurry microstructures from the ultrasonically measured data.

4.2.3 The inverse characterisation of microstructures. Ultrasound has been widely employed to characterise the solid concentration, PSD, dispersion and homogeneity in suspension systems. This inverse problem is typically solved through model-based iterative fitting,[205] by assuming a predefined particle size distribution shape – commonly log-normal – and fitting key parameters (*i.e.* mean and standard deviation) to the experiments data. This section samples the relevant literature on dense slurries; the actual applications likely far exceed what is covered below, because many are proprietary to industrial companies and thus not disclosed.[40] It is worth pointing out again that very few examples have a viscoelastic composite structure similar to battery slurries.

most common characterisation of slurry microstructures is to extract PSD and concentration using UAS, as shown in Fig. 10(a). Good agreement of PSD results is demonstrated in Fig. 10(b) between those obtained by ultrasonic attenuation and by a commercial laser diffraction-based particle sizing instrument, for cases of an oil-in-water emulsion and a low-concentration aqueous suspension of glass beads.[40] Hipp *et al.* also achieved similar results on monidisperse silica suspensions and PTFE suspensions of different particle sizes at different weight concentrations using the core–shell model,[195] shown in Fig. 10(c). Stolojanu and Prakash characterised concentration and PSD in aqueous glass beads slurry with up to 45 vol%.[206] Bamberger and Greenwood used real-time ultrasonic attenuation to monitor slurry concentration during mixing,[207] see Fig. 10(d). Falola *et al.* addressed the challenges and respective importance of unknown physical properties,[208] which is relevant because some properties of battery slurry are unknown.

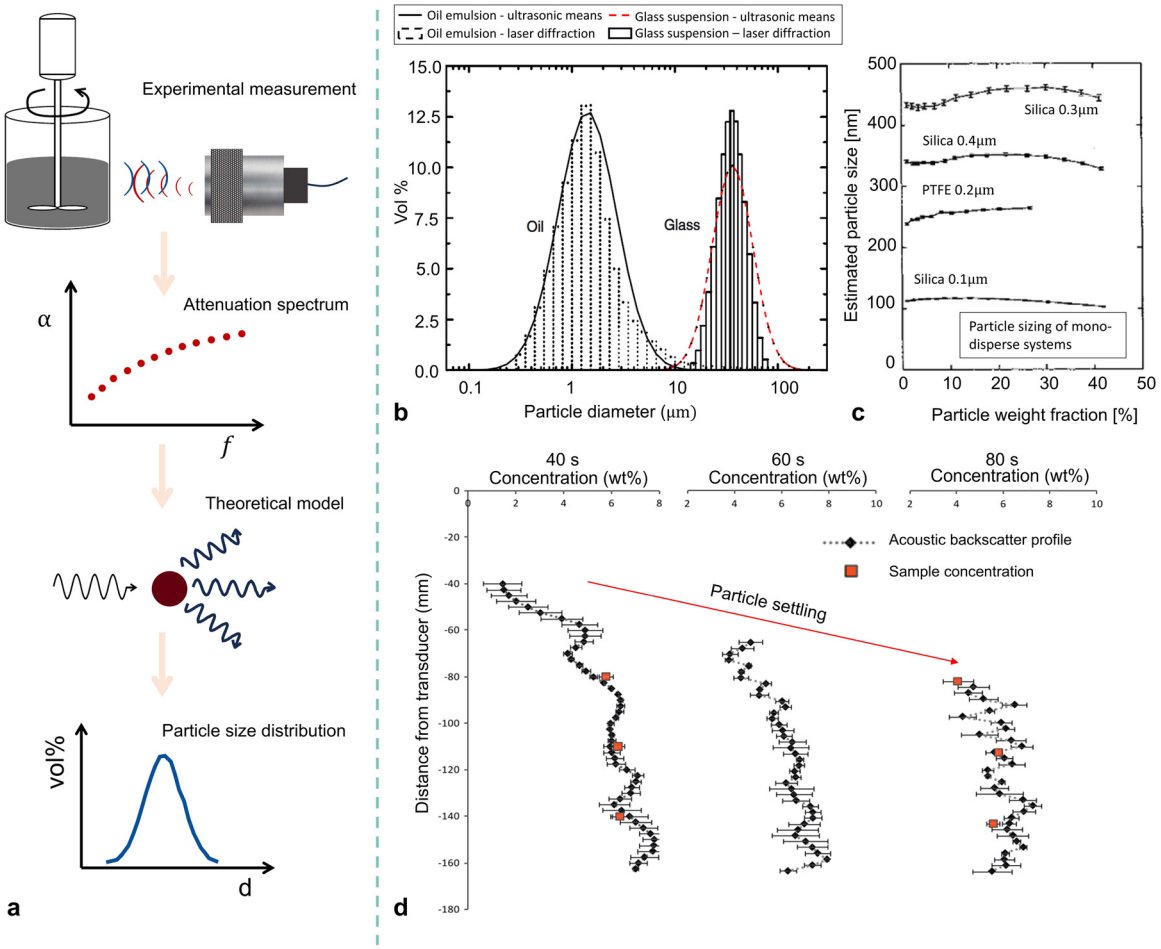

Fig. 10 The inverse characterisation of microstructures from UAS measurement. (a) The working principle of the inverse process; (b) PSDs obtained from ultrasonic means compared to laser diffraction for oil-in-water emulsion and aqueous suspension of glass beads. Reproduced with permission from ref. 40. Copyright 2005, Institute of Physics Publishing. (c) Particle sizes (d_{50}) of different mono-disperse suspensions over a range of concentrations. Reproduced with permission from ref. 195. Copyright 2002, American Chemical Society. (d) Concentration profile measurement of a settling flocculated spheriglass dispersion at 40, 60, and 80 s measured by Acoustic Backscatter System (ABS). Reproduced with permission from ref. 209. Copyright 2012, Elsevier Ltd.

Backscattering analyses are also used. Burgess *et al.* compared optical & ultrasonic attenuation against backscattering methods on high-level waste up to 40 wt%, and found good agreements.[210] Greenwood estimated PSD and density of a slurry using backscattering from a solid interface.[176] Weser *et al.* demonstrated a strong correlation between backscattering and particle concentration gradients, enabling real-time tracking of settling dynamics.[175,204] Lombard used parameterised backscattering coefficient to study the effects of shear-induced anisotropic microstructures.[211]

Characterisation of homogeneity and dispersion can be viewed as derivatives of the PSD characterisation, since aggregation or flocculation of particles result in larger detectable particle sizes. Cavegn *et al.* demonstrated that ultrasonic resonances of the particles can sensitively trace the homogenisation evolution of nanoparticulate pharmaceutical vehicles.[212] Tonge *et al.* used backscattering to study the flocculation in complex waste and noted the importance of *a priori* system data on the accuracy of the acoustic method.[213] Fig. 10(d) shows the concentration profiling of a settling flocculation measured through backscattering, suggesting its capability of real-time monitor of system homogeneity during dynamic process.[209]

4.2.4 Research gaps on characterising microstructures. While ultrasonic characterisation of particle statistics are well-established for various suspension systems, their successful application to battery slurries requires addressing several important research gaps, which arise from the unique and complex microstructures of battery slurries.

The primary research gap is to incorporate the viscoelasticity of the continuous phases. As highlighted in Section 4.2.1, the polymeric binders create a surrounding medium that can significantly store and dissipate wave energy through frequency-dependent relaxation mechanisms. Given that the way ultrasound interacts with the suspended particles is fundamental to a scattering theory, this is a notable difference from the Newtonian continuous phase commonly assumed by the ECAH-based models[44,45] and related experimental work. Although models considering viscoelastic particles[214] or extending the ECAH model to viscoelastic emulsions[215] exist, the research gap is to develop or adapt forward models that can adequately account for the specific constitutive behaviour – which is conceptually not difficult and could be achieved by using complex, frequency-dependent material properties – and investigate the resulting interaction mechanisms in battery slurries.

Further complexities arise from the inherent microstructures in battery slurries. These include high solids concentration ($\sim$20–25 vol% for NMC cathode slurries, and $\sim$25–40 vol% for graphite anode ones[80]), often near the validated limits of multiple scattering models. Additionally, the flake-like morphology of graphite particles[216] in anodes deviates from the spherical–particle assumption and scattering behaviours in standard ECAH models. Moreover, the polydispersity of these slurries (*i.e.* they consist of multiple particle species, and the AM and CA have vastly contrasting sizes[28,35]) poses interesting problems for the classic models, which in principle can accommodate multiple species, but it is worth investigating whether important physics that is typically not accounted for in these models (*e.g.* direct particle interactions, entanglement) can be separated and determined from the ultrasonic data. These factors require extensions to ECAH models, or alternative approaches like EMTs, CPMs, MCMs to better approximate the ultrasonic wave propagation.

Finally, the efficacy of ultrasonic characterisation is highly dependent on model parametrisation and the robustness of the inversion algorithm. Forward models like ECAH require numerous physical properties of the constituent phases, many of which may be unknown or dependent on specific battery materials, and such uncertainties can significantly affect the accuracy of forward prediction and inversion. Mitigation methods include sensitivity analyses to determine the most significant parameters,[174,217] and incorporating unknown properties in the fitting process,[218] but more systematic solutions are needed. Furthermore, extracting the detailed microstructural information from the ultrasonic attenuation spectra, which are often featureless, may pose an inherently ill-posed problem prone to non-unique solutions. This requires robust optimisation techniques and strategies to supplement the input information, such as measurements over wider frequency ranges, though this presents experimental and cost challenges, particularly at higher ($>$20 MHz) frequencies.[40]

The points above only considered a snapshot state of the slurries as an isolated and static one, but the dynamic evolution of slurry microstructure during mixing presents another set of challenges and opportunities, particularly in tracking the progress towards the desirable homogeneous state. The size of aggregates and agglomerates can be monitored as crucial indicators of the dispersion process by exploiting the multi-mode particle resonances:[219] the typical 50–80 μm aggregates[28] have resonant frequencies well within the 20 MHz working range of common ultrasonic setups. Importantly, this approach has already been proved effective in other industries.[212,213]

As an example, this may allow real-time evaluation of the spatial binder distribution and the formation of the CBDs, which are critical for electrode performance[29,220] (see Section 2.1.1) but are currently a significant challenge for direct characterisation, even using offline techniques. The evolution of carbon-binder network distribution, from initial aggregates to the evenly distributed state,[114] would likely alter particle resonances and viscoelasticity of the continuous phase, both of which can contribute to detectable wave characteristics. As such, ultrasonic indicators could be developed to track the effectiveness of binder distribution and the overall maturation of the slurry CBD. This represents a research opportunity to realise inline characterisation of one of the slurry's most important yet elusive properties.

4.3 Ultrasonic measurements of macroscopic properties

Beyond microstructures, ultrasonic techniques hold promise for the *in situ* determination of some macroscopic rheological properties of battery slurries, notably viscosity and viscoelasticity, which are examined in this section, along with challenges and research gaps for applications on battery slurries. Ultrasound cannot directly access properties like yield stress or extensional rheology.

4.3.1 Viscosity. Viscosity quantifies a fluid's resistance to deformation under applied stress, particularly shear. There are

two widely adopted ultrasonic techniques to estimate this property: shear wave reflectometry and guided wave viscometer, see Fig. 11(a) and (b).

Shear wave reflectometry relies on the principle of viscous coupling at a solid–fluid interface. When a shear wave is incident upon a solid–fluid interface from the solid side, part of its energy is transmitted through to the fluid, resulting in amplitude drop and phase shift to the reflected wave, which are dependent on the fluid's viscosity. The mathematical equations to calculate shear viscosity from the measured complex reflection coefficient are presented in Appendix D. Since originally proposed by Mason *et al.*,[221] this method has been widely adopted to measure various fluids,[48,222,223] including lubricant oils[224] – see Fig. 11(c) – and many other types of lubricant contacts.[225] This technique generally works better on high-viscosity fluids, since the reflection coefficients of low-viscosity one are close to unity due to weak coupling, making the small changes in amplitude and phase difficult to resolve.

Guided wave viscometries also exploit the viscous coupling of the shear or torsional modes fundamentally. When a waveguide (*e.g.* a dipstick) is immersed in the slurry, the propagating wave leaks energy into the surrounding fluid, and the resultant attenuation is quantitatively related to viscosity,[226] see Fig. 11(e). Unlike reflectometry, where shear rate is dictated by wave frequency and amplitude, guided wave techniques offer additional control and design space through waveguide geometry. Various configurations have been demonstrated, including shear-horizontal waves in dipsticks,[227] torsional waves in rods,[228,229] and Lamb waves in thin sheets.[60] Additionally, waveguides offer improved spatial sampling, as they can be repositioned to probe viscosity at different locations.

It is important to recognise that most of the above applications are for Newtonian fluids. For non-Newtonian battery slurries, the goal is to characterise viscosity across a range of shear rates. However, ultrasonic methods – reflectometry[224] or guided wave-based[60,228] – consistently report lower viscosities than conventional rheometers, as shown by comparisons between Fig. 11(c)–(f). Several explanations have been proposed to reconcile the differences. Peretti *et al.*[224] suggest that ultrasound probes high-frequency, small-strain behaviour, equivalent to shear rates around 10^6 s^{-1}, and rely on the Cox–Merz rule[230] to relate complex viscosity $\eta^*(\omega)$ to steady-shear viscosity $\eta(\dot{\gamma})$. This interpretation aligns with the lower values observed at higher shear rates for shear-thinning fluids. In sharp contrast, however, Kazys *et al.*,[60] using finite element modelling, estimated wave-induced shear rates to be <1 s^{-1}, attributing the low viscosity readings to viscoelastic relaxation rather than high shear. These conflicting interpretations highlight a key unresolved issue: the effective shear rate in ultrasonic measurements remains ill-defined, and bridging the gap between dynamic and steady-shear viscosity remains a critical theoretical and practical challenge.

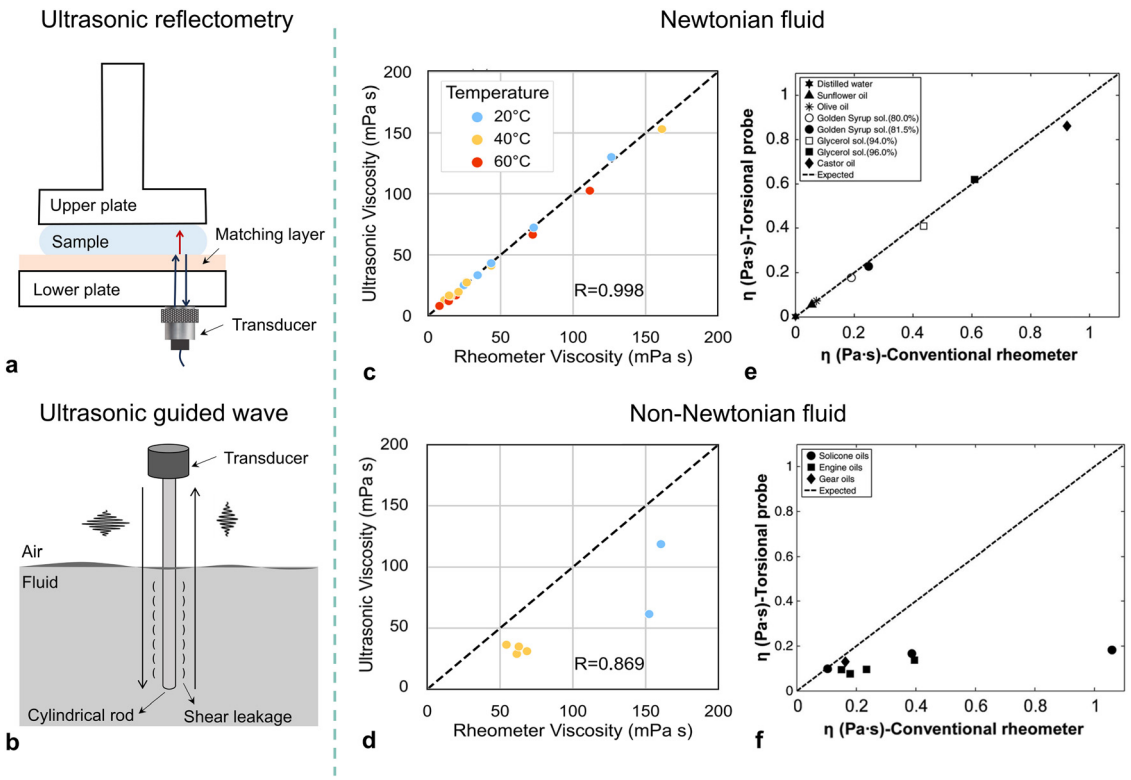

Fig. 11 Ultrasonic measurement approach for fluid viscosity. (a) An illustration of shear wave ultrasonic reflectometry (redrawn based on ref. 224); (b) a schematic of a guided wave measurement setup in torsional mode (redrawn based on ref. 228); (c) and (d) a comparison of viscosity measured from ultrasonic reflectometry and conventional rheometer for Newtonian-like lubricants and Non-Newtonian fluid respectively. Reproduced from ref. 224. Copyright 2024, licensed under CC BY 4.0, Elsevier Ltd. (e) and (f) A comparison of viscosity measured from conventional rheometer and the torsional waveguide probe for Newtonian fluid and Non-Newtonian fluid respectively. Reproduced from ref. 228. Copyright 2011, licensed under CC-BY-NC-ND 4.0, Institute of Electrical and Electronics Engineers.

In addition, the UVP-PD (Ultrasound Velocity Profiling-Pressure Drop) technique[231,232] combines velocity profiles in pipe flow with pressure drop measurements across a defined length, to determine local shear rates and shear stresses, and derive rheological properties. The method is well established and has in fact been applied to monitor battery slurries during post-mixing transport,[38] but it is not suited for real-time optimisation of the mixing process itself.

4.3.2 Viscoelasticity. Viscoelasticity characterises battery slurry's simultaneous liquid-like viscous and solid-like elastic responses to external stress (note that all viscoelastic fluids are non-Newtonian). As reviewed in Section 2, it originates from the microstructures and influences the slurry's stability and processability in the coating and drying steps. The objective of characterising viscoelasticity is to determine the frequency-dependent moduli $G'(\omega)$ (representing elastic energy storage), and $G''(\omega)$ (representing viscous energy dissipation).

Shear wave reflectometry can be extended to determine viscoelastic properties. By propagating obliquely incident shear-horizontal waves to an interface between a known and the target materials, as in Fig. 12(a), G′ and G'' can be calculated from the frequency-dependent magnitude and phase of reflections (see Appendix D). Alig *et al.*[233] integrated digital signal processing to Mason's original method, enabling frequency- and time-resolved measurements of the complex moduli of polymer films during dynamic film formation and crystallization. Wang *et al.*[234] used this approach to track the evolution of G' and G'' during cement paste hydration, where the moduli changed significantly, as shown in Fig. 12(b). Rabbani and Schmitt[235] applied it to measure the viscoelastic moduli and viscosity of ultra-heavy non-Newtonian bitumen.

The more common ultrasonic characterisation of viscoelasticity is through the frequency-dependent speed and attenuation of propagating bulk elastic waves. One prominent application is shear wave-based medical imaging, from the early work on elastography[236,237] which focused on the elastic storage modulus, to the subsequent development of Shear wave Dispersion Ultrasound Vibrometry (SDUV) which incorporated viscosity.[238,239] The methodology is now widely used to measure viscoelasticity in liver[240] and other soft tissues.[241] Beyond medical applications, Larcher *et al.*[242] used compressional wave speed and attenuation to determine the complex modulus of asphalt across temperature and frequency ranges, and Letang *et al.*[243] combined through-transmission compressional waves with shear wave reflectometry to measure the moduli of wheat flour-water doughs.

These studies share similar fundamental procedures. The first step is to select an appropriate wave mode and obtain its frequency-dependent propagating parameters. Shear waves are preferable where they exist (*e.g.* in soft tissues), since they are directly linked to the viscoelastic moduli.[237,239] For slurries, which cannot sustain propagating shear waves, compressional waves can be used instead, though they only offer indirect and

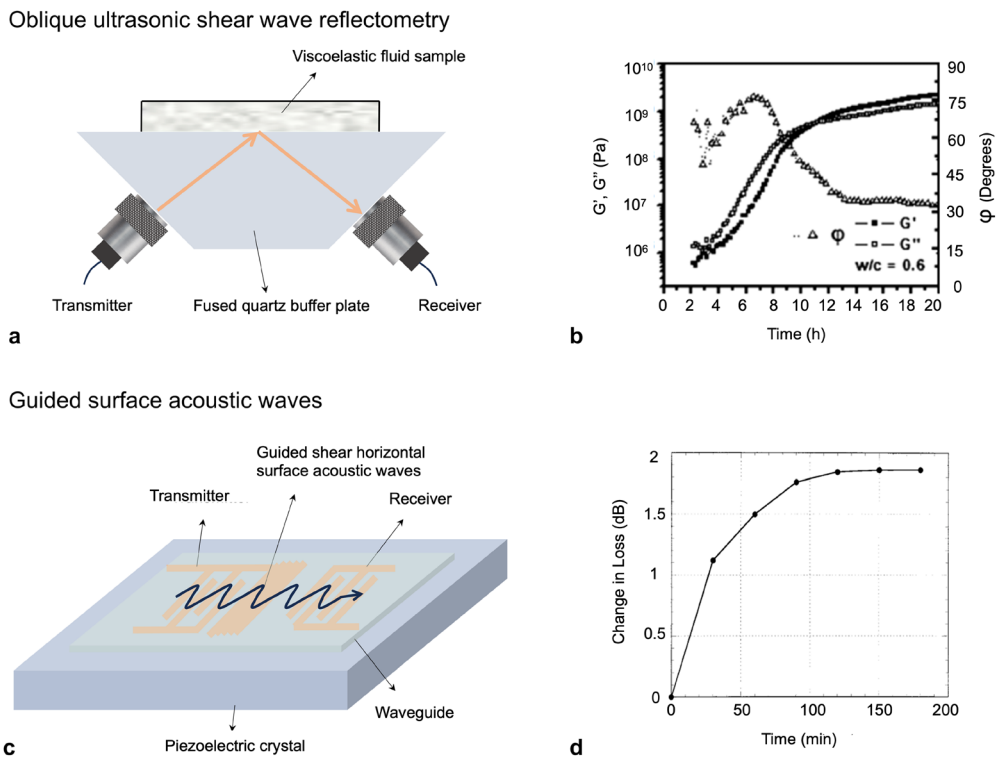

Fig. 12 Ultrasonic measurement approach for fluid viscoelasticity. (a) An illustration of obliquely incident ultrasonic shear wave reflectometry (redrawn based on ref. 234); (b) G', G'', and phase of shear modulus φ as a function of elapsed time during cement paste hydration at 1 MHz for water-to-cement ratio equals to 0.6. Reproduced with permission from ref. 234. Copyright 2010, Elsevier Ltd. (c) An illustration of guided shear horizontal surface acoustic wave (SH-SAW) measurement setup (redrawn based on ref. 247); (d) changes in SH-SAW energy loss as a function of curing time for a 2 μm thick PMMA coating, which is an indication of the viscoelasticity change. Reproduced with permission from ref. 247. Copyright 2001, American Chemical Society.

less sensitive evaluations.[242] To overcome this, guided wave modes involving localised shear motion have been explored, for example Lamb,[244] Rayleigh,[245] Love[246,247] and shear horizontal[248,249] waves, especially the latter two types which are dominated by shear motion. Fig. 12(c) demonstrates a guided shear horizontal surface acoustic wave (SH-SAW) measurement setup and Fig. 12(d) shows the changes of acoustic energy loss during dynamic curing process, which serve as an indicator of the viscoelastic properties. However, these waves propagate within the waveguide and its vicinity, not the bulk of the slurry itself, making the waveguide geometry critical for maximising shear interaction and sensitivity. Limitations such as finite boundary conditions and mode overlap must also be carefully considered.[245]

The second step involves selecting an appropriate viscoelastic model. The choice should reflect the material's expected mechanical behaviour. While simple models like Voigt and Maxwell are useful for medical ultrasound,[239,250] they likely cannot capture the complex, multi-timescale relaxation behaviour of battery slurries.[80,86] The generalized Maxwell model (GMM),[251] which includes multiple Maxwell elements in parallel, may offer a better fit, though the model complexity and physical interpretability must be carefully balanced.[252]

Finally, the frequency-dependent experimental parameters (*e.g.* wave speed and attenuation) are fitted to the chosen model using numerical optimisation techniques, typically non-linear least squares,[245] to extract the viscoelastic parameters that best describe the material.

Even though the reviewed techniques are well-established for characterising viscoelasticity in soft tissues and various non-Newtonian fluids, their effectiveness on battery slurries is not guaranteed. This is partly due to the complex microstructures of such slurries, and partly the inherent limitations of the techniques themselves, such as sensitivity and robustness of inversion. These challenges and associated research gaps for measuring both viscosity and viscoelasticity are discussed next.

4.3.3 Research gaps on measuring macroscopic properties. As mentioned in Section 4.3.1, a primary research gap is the interpretation of ultrasonic and steady-state measurements of dynamic viscosity in non-Newtonian slurries, where the underlying reasons for discrepancies remain unclear.[228,235] It is important to rigorously determine the shear rates that the ultrasonic measurements actually probe, and the applicability of empirical relationships like the Cox–Merz rule,[230] which attempts to correlate dynamic viscosity with steady-shear viscosity, needs systematic re-evaluation. However, regardless of the outcome, it should be made clear that ultrasound can only measure viscosity in a very limited shear rate range, determined by its frequency, amplitude and waveguide geometry (for guided waves), unlike rheometers which can operate within a continuous and broad range of shear rates.

For viscoelasticity measurements, the selection of appropriate wave modes remain crucial, given that battery slurries do not support long-range propagation of shear waves. While propagating compressional waves can be used,[242] they are often based on similar experimental setups with microstructural characterisation and data (*e.g.* compressional wave attenuation spectra). To fit both the microstructures and macroscopic rheology with the same data is not ideal, as the sensitivity to each differs and the inversion problems may become intertwined.

Shear wave reflectometry and guided waves can diversify the ultrasonic data source and provide direct sensitivity to both viscosity and viscoelasticity. In particular, guided wave sensors offer design space (*e.g.* wave modes, waveguide geometries, and frequencies) that should be systematically explored to optimise their sensitivity, and to achieve more robust measurements of parameters relevant to slurry processability. Thanks to their different data sources, guided wave measurements also present an opportunity to integrate their macro-rheological results to the microstructural interpretation models for improved accuracy. For instance, the measured viscoelasticity could serve as feedback or constraints of the continuous phase in the scattering models. However, a concern about these techniques is that they are interface-based, and they primarily probe a thin slurry layer adjacent to the surface of the sensor or waveguide. Whether this thin-layer measurement is truly representative of the bulk slurry properties needs further investigation, especially given the complex boundary conditions such as binder attachment to surface or localised structuring near boundary.

For the modelling of viscoelasticity, while the GMM is suitable for capturing the broad relaxation spectra of battery slurries, a significant gap is to robustly parametrise and fit GMMs from ultrasonic data. Determining the optimal number of Maxwell elements to ensure both fitting accuracy and physical interpretability is challenging,[253] and development should focus on establishing standard protocols and validation methods for these purposes.

It is also important to note that many ultrasonic measurements, particularly those involving shear waves or guided waves, are sensitive to not the viscosity itself, but often the product of density and viscosity.[254] Many of the viscosity measurements reviewed previously assumed constant density, but this may not hold true during battery slurry mixing. While density itself is not a rheological property, it is important for accurately decoupling viscosity or viscoelasticity. Thus, developing methods for simultaneous or independent ultrasonic density measurement could be beneficial.

Finally, as an opportunity, the existing and to-be-developed guided wave frameworks for the characterisations of viscosity and viscoelasticity could find applications beyond slurry mixing, in monitoring the coating and drying steps of electrode manufacturing. The transition from a liquid slurry to a solid-like porous electrode involves significant changes in viscoelastic properties, which guided waves are well-suited to track, potentially offering new avenues for inline quality control of these critical downstream processes. In fact, there have already been relevant experimental developments using air-coupled ultrasound techniques.[255,256]

5 Perspectives on inline ultrasonic monitoring of battery slurries

Towards the goal of reducing scrap in battery slurry mixing, an inline characterisation technique serves two purposes: as a

direct feedback mechanism for parameter optimisation during production ramp-up, and as conformance assurance when production is running at capacity. For both purposes, the measurements should be conducted *in situ*, and ultrasonic techniques presents notable advantages.

As reviewed, ultrasonic wave's attenuation, velocity, and backscattering are sensitive by microstructures; the evolution from the initial state full of aggregates and agglomerates, to the ideal state with evenly distributed binder and CA networks, could likely result in detectable changes of ultrasound and thus allow the evolution itself to be monitored. These are significant, because such parameters are deterministic to downstream product performances and yet elusive to existing techniques. Moreover, ultrasonic instruments are easily available, non-invasive, and well-suited for integration into industrial production environments, offering a viable pathway toward real-time monitoring.

Despite these advantages, several limitations constrain the use of ultrasound as a standalone characterisation tool. These include the research gaps already identified, and the fact that ultrasound's access to certain properties are limited and indirect. For example, it struggles to capture specific microstructures (*e.g.* chemical surface interactions) and key macroscopic rheological behaviours (*e.g.* viscosity at only limited shear rates, extensional rheology, and yield stress), all of which are important to evaluating slurry processability. Consequently, a new strategy is needed to make full use of the valuable yet limited information accessible by ultrasound.

5.1 Bridging microstructure and rheology with predictive modelling

Since bulk rheological behaviour directly determine slurry processability, and ultrasonic techniques are better suited for inferring microstructural features than directly capturing rheological parameters, a logical approach is to use ultrasound for inline microstructure characterisation, and feed the information to predictive modelling (reviewed in Section 3.2) to estimate the rheological properties. While different strategies implement this workflow in various ways, they can generally be grouped into three categories: physics-based models, multi-scale simulations, and data-driven or machine learning (ML) approaches.

5.1.1 Existing predictive frameworks. Physics-based models can be integrated in two steps: initially, microstructural information (*e.g.* PSD, concentration) is extracted from inline ultrasonic data using the scattering or effective medium theories discussed in Section 4.2.2. Subsequently, these parameters can serve as inputs to the micro-rheological models (detailed in Section 3.2) to predict macroscopic rheology, which can be further validated by the limited ultrasonic viscosity and viscoelasticity data. However, the primary challenge of this approach is the potential error propagation: ill-posed ultrasonic characterisation of the slurry's microstructures (which result from the existing research gaps) can compound uncertainties within the micro-rheological models themselves (*e.g.* particle properties and the mechanistic descriptions of interaction mechanisms). Consequently, while this approach may yield useful trends, the overall predictive accuracy is expected to be limited.

Multi-scale simulations such as CGMD and DEM (reviewed in Section 3.2) provide a powerful framework to link fundamental particle interactions to rheology. However, this only solves one step of the problem; full-field numerical simulations (*e.g.* finite element methods) to link slurry microstructures to bulk ultrasonic responses presents a significant technical challenge. This is primarily due to the extreme disparity in length scales, from micron-scale scatterers to centimetre-scale propagation domains, making this approach infeasible for real-time or inline monitoring of slurries. A more practical route involves using effective medium theories[196] to approximate ultrasonic behaviour in complex suspensions, and employing CGMD or DEM simulations to generate synthetic microstructure–rheology datasets for training physics-informed surrogate models that bridge ultrasonic features and slurry states.[168]

Data-driven and ML models enable directly correlating ultrasonic features with the targeted rheological properties from large datasets, potentially bypassing the intermediate step of explicit microstructure inversion. Complex, non-linear relationships can be captured this way. However, their successful application is critically dependent on the availability of extensive, high-quality calibration data[257] linking ultrasonic responses to verified slurry properties, and they share the general ML challenges of potential overfitting and limited extrapolation capability beyond the training data.[258]

5.1.2 Physics-informed ML models and PINNs. Physics-informed ML models (PIML) frameworks address key limitations of purely data-driven models by embedding physical knowledge into the ML models.[61] In simpler terms, rather than just learning from data patterns alone, these models are also 'taught' by the fundamental laws of physics relevant to the problem. Among them, physics-informed neural networks (PINNs)[259] are particularly promising for inline ultrasonic characterisation of battery slurries. A PINN is a type of neural network that embeds physical laws (such as the equations governing wave propagation or fluid dynamics) directly into the neural network's learning/training process, typically by expressing the residuals of governing equations or other mathematical constraints as part of the loss function. This physics-informed regularisation guides the learning process, and forces the PINN's predictions to be not just data-consistent, but physically realistic. As a result, PINNs can effectively solve ill-posed inverse problems and make robust predictions, even with sparse or noisy experimental data. PINNs also gains great flexibility, and the physical layer can integrate not only partial differential equations (PDEs) like the wave equation, but also empirical relationships, material constitutive models, or dynamic state-space equations. These advantages have seen PINNs gaining widespread adoption across physical sciences and engineering,[260–262] including in ultrasonics.[263,264] Therefore, we believe that a combined approach of inline ultrasonic measurements + PINN-based predictive modelling represents the best way forward, overcoming the limitations of physics-only or purely data-driven models.

In the context of ultrasonic monitoring of battery slurries, three key layers of physical knowledge can be integrated into a

PINN. First is the analytical wave propagation and scattering models which links the slurry microstructures to ultrasonic characteristics (attenuation, speed, and scattering), such as ECAH, core–shell or effective medium theories, as discussed in Section 4.2.2. Second, relationships between microstructure and rheology, as described by empirical (*e.g.* Herschel–Bulkley[152] or Krieger–Dougherty[153] equations) or micro-rheological models[87] can be incorporated to to predict rheological behaviours from the ultrasonically inferred or physics-constrained microstructural state. A third layer can utilise direct correlations between specific ultrasonic features (*e.g.* reflection coefficient) and rheological parameters like viscosity and viscoelasticity. Each physical layer in this multi-layer integration contributes to the overall loss function of the PINN, so that the complex, multi-domain relationships can be learnt, and predictions that are both data-consistent and physically coherent can be produced. It is crucial to recognise that the fidelity of these embedded physical layers is fundamental to the efficiency and accuracy of the PIML/PINN model; as such, continued research to advance the fundamental understanding and to bridge the research gaps identified in Section 4 remains of paramount importance.

There are also technical challenges facing such applications. Potential limitations of PINNs[61] include spectral bias against high-frequency details crucial for fine microstructural characterisation; difficulties in handling coupled multi-physics and multi-scale inherent in the polydispersive slurries; and sensitivity to the noise and sparsity often present in inline experimental data. Fortunately, the broader field of PIML is rapidly evolving, with ongoing research providing potential remedies. For instance, Fourier feature mapping or adaptive activation functions can mitigate spectral bias,[263,265] specialised architectures like DeepM&M[266] show promise for complex multiphysics and geometries, and Bayesian PINNs[267] offer robust uncertainty quantification to handle data imperfections. Beyond these direct PINN enhancements, the PIML landscape is rapidly progressing through innovations such as operator learning frameworks (*e.g.* DeepONets,[268] Fourier Neural Operators[269,270]), or Laplace operator,[271] which learn mappings between function spaces. Thus, while PINNs currently represent a pertinent and extensively researched methodology suitable for the combined inline ultrasound + predictive modelling approach, even more specialised and powerful tools may be on the horizon.

5.2 Roadmap to implementation

5.2.1 Model calibration and PINN training. The accuracy of the proposed combined approach hinges on robust offline calibrations, which can integrate state-of-the-art measurement techniques, modelling insights, and physical laws into the unified learning framework of PINNs.[61,259] In practice, the calibration process could start by preparing a matrix of slurry formulations with systematically varying mixing configurations, such as solid loading, binder content, mixing sequence and duration. A good strategy to minimise the required number of samples is the design of experiments method used in ref. 166. Each slurry sample undergoes ultrasonic measurements under controlled conditions, alongside extensive offline characterisations with the range of techniques as reviewed in Section 3. The resulting dataset captures a detailed and comprehensive snapshot of each slurry's microstructure–rheology-ultrasound relationships.

The calibration dataset provide paired inputs and targets for the PINN to learn mappings from real-world ultrasonic signals to latent slurry properties, while remaining anchored by the physical principles,[263] see Fig. 13(a). The three physical layers are embedded in the model through the construction of a composite loss function, which typically includes terms that enforce agreement with the empirical calibration data, as well as residual penalties for violating the governing equations of ultrasonic wave propagation and the constitutive relations of the slurry medium. Such a structure ensures that the learning process remains consistent with both data and physics, even when the former are sparse or noisy.[61,259] The PINNs can be trained on a combination of simulated and experimental data,[272] and an effective training strategy is to first pre-train or constrain the PINN with physics alone on a wide range of slurry states. This can be done by predicting ultrasonic features from the physics models – once they are developed to a state where they can capture the characteristics of the battery slurries with high fidelity – across various microstructure parameters to create a synthetic dataset. The network will learn a physics-valid, albeit rough, mapping from this step. Then the PINNs can be fine tuned on real experimental data, which do not need to cover all conditions densely, since the implemented physics allow reliable interpolation.[262] The result is a model that accurately interpolates the real data and extrapolates to new conditions allowed by physics.

Once trained, the PINN can be deployed as a surrogate model to interpret incoming ultrasonic data in real time, delivering estimations of slurry conformance, microstructure, and rheology. Because the model has been trained to obey both experimental observations and physical laws, it can provide robust predictions with signal variability or partial data loss.[61] The computation is fast, since it is essentially a forward pass through the neural network. The PINNs can also be adaptive, using the data accumulated from continuous running to periodically re-train or update the model and effectively construct a digital twin of the inspected system.[61] These advantages make it a feasible and robust option for closed-loop optimisation and real-time monitoring of the mixing process, as illustrated in Fig. 13(b).

It is worth highlighting the power of this PINN approach, which lies in its ability to effectively incorporate the extensive offline characterisation techniques. The fully trained PINN serves effectively as an advanced data fusion tool for the rich information gathered from all the offline measurements, and the inline ultrasonic signals acting simply as real-time pointers to the comprehensively characterised, multi-dimensional slurry states. This is a sharp contrast to the purely physics-based models, which infer the complex properties solely from ultrasonic signals and often face limitations due to the indirect measurements and ill-posed nature of the relevant inversions.

5.2.2 Sensor selection and deployment. The inline ultrasonic monitoring system requires careful consideration of

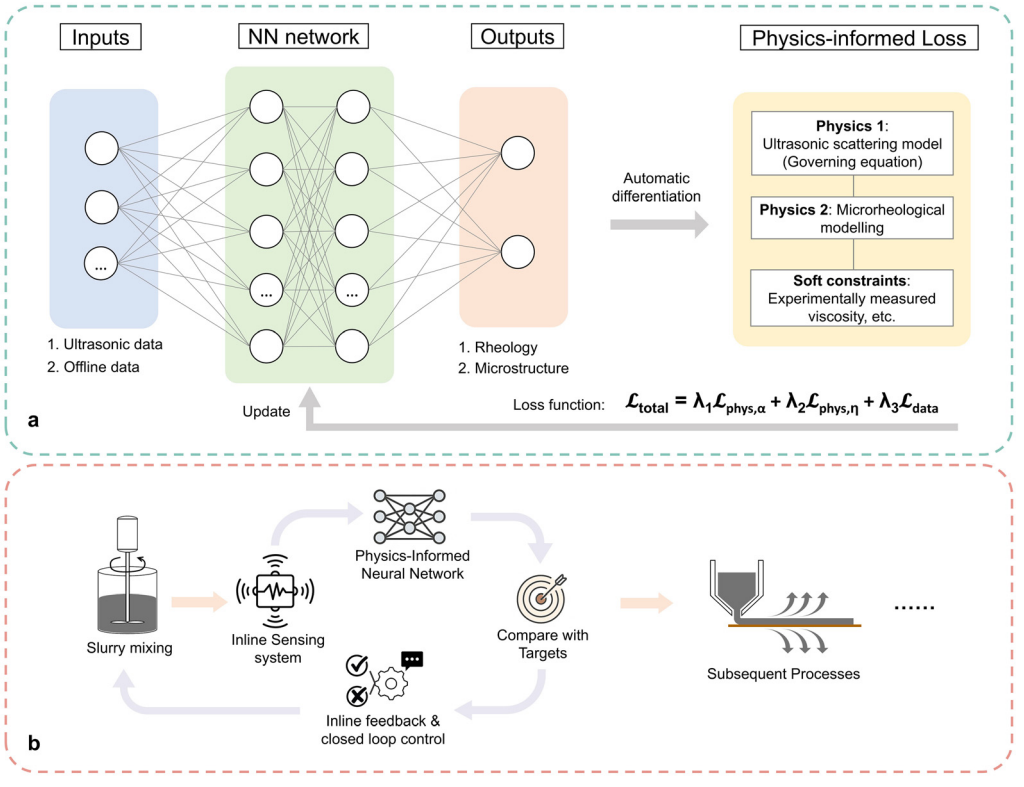

Fig. 13 Perspectives on inline monitoring of battery slurries using a combined ultrasonic monitoring + PINN-enabled prediction approach. (a) Schematic of the proposed physics-informed neural network (PINN) architecture; (b) the vision of closed-loop optimisation and control of battery slurry mixing enabled by the combined approach.

instrumentation and its integration to the process control of slurry mixing. A key consideration is the choice of ultrasonic transducers – their type, operating frequency and mode,[40] and each chosen transducer must be clearly tailored to measuring its targeted slurry properties. The data fusion capabilities of PINNs relax the stringency of the choices;[61,259] in fact multiple sensors are advantageous as input to PINNs over a single one, as long as they deliver diverse data. For macroscopic rheological properties, shear wave reflectometry uses pulse-echo setup with broadband excitation,[221] whereas guided wave viscometry require careful design on the waveguide geometry.[227,228] For microstructures, a balance should be sought between propagation length, resolution, and sensitivity to the fundamental physical mechanisms at play. These are best implemented using broadband transducers in the 1–20 MHz frequency range.[40,172] One aspect to be careful about battery slurries is that they normally have high attenuation and thus short propagation distances at higher frequencies,[183] which necessitate narrow measurement gaps; but the high viscosity can lead to sensor fouling in confined gaps. Therefore, instrumentation must not only accommodate the acoustic characteristics of the medium but also be mechanically robust and easily cleanable.

The integration of ultrasonic sensors to the mixing devices must ensure that the ultrasound path samples representative bulk material. Backscattering measurements may be conducted through the mixer's wall, but attenuation sensors should be in direct contact with the slurry and ideally embedded in the mixing vessel[207] while avoiding stagnant regions. Sensor mounting should also accommodate the need for mitigating sensor fouling, and be isolated from mechanical movements and vibrations of the mixer components. One important consideration is that temperature measurement and compensation are essential to ultrasonic tests, as the wave velocity and attenuation are sensitive to thermal perturbations.[177]

To integrate into process control systems, inline ultrasonic measurements of microstructures and macro-rheology need to be synchronised with the mixing operations and streamed to a controlling unit. The inference model (PINNs as proposed here) should operate within an acceptable latency level, and its outputs, including viscosity estimates or dispersion quality indicators, can then inform the decision making process and used as input to closed-loop control strategies.[38,110] These may lead to real-time adjustments of mixing speed, duration, or additive dosing, thus improving slurry product conformance and batch-to-batch consistency, and transforming slurry mixing from a heuristics-based process into a data-informed and adaptive one that is anchored by real-time physical insight.

6 Summary and outlook

The soaring demand for batteries, which is pivotal in the global transition to sustainable energy, is significantly hampered by

manufacturing inefficiencies, particularly in the critical slurry mixing stage. High scrap rates at this juncture are caused by the reliance on slow, offline characterisation methods and the resultant open-loop control, resulting in substantial material waste, economic losses and environmental impacts. This paper has critically examined the largely untapped potential of low-power ultrasonic techniques to provide robust, inline monitoring of battery slurry mixing, thereby addressing this pressing industrial need.

We began by detailing the crucial microstructural characteristics (*e.g.* particle size distribution, homogeneity, dispersion and binder distribution), and macroscopic rheological behaviours (*e.g.* viscosity and viscoelasticity) that dictate slurry processability and ultimate battery performance. The complex interplay of numerous mixing parameters makes optimising these properties a formidable challenge for the existing offline characterisation tools, which impede rapid, data-driven feedback for process control. This review introduced the fundamentals of ultrasonics, and highlighted how the interactions between waves and slurry constituents, manifested as changes of wave speed, attenuation and scattering, can be used to characterise the vital slurry parameters. Despite facing unique challenges posed by battery slurries, such as high solids content, polydispersity, and the viscoelastic nature of the continuous phase, ultrasound's potential for inline microstructural and limited rheological evaluation remains significant.

To overcome the limitations of ultrasound as a standalone tool for battery slurries, and to bridge the gap between measurable ultrasonic parameters and the suite of desired macroscopic rheological properties, we proposed a synergistic strategy. This approach involves integrating inline ultrasonic data with predictive modelling frameworks, particularly physics-informed neural networks (PINNs). By embedding the governing physical laws of ultrasound-microstructure-rheology relationships into the PINNs training process, and leveraging comprehensive offline calibration datasets and optimised instrumentation, this methodology points to a clear pathway where real-time estimation of slurry properties can be inferred from inline ultrasonic data continuously. Once integrated to the control system, this system can enable true closed-loop optimisation and dynamic adjustments of configurations, heralding a leap towards more efficient and sustainable battery manufacturing.

The implications of this combined ultrasound-PINN methodology extend beyond wet LIB slurry mixing. For example, they could be applied to monitoring the slurries of sodium- and zinc-ion batteries, which are very similar to LIBs. Furthermore, as the industry explores innovative manufacturing routes such as dry electrode mixing,[273] there are significant challenges in monitoring the evolution of particulate blending and binder fibrillation. The ultrasound-PINN framework offers a viable monitoring path: the propagation of ultrasound can probe the evolving microstructure, from the initial particulate powders[274] to the final state of porous solids,[275,276] and PINNs can integrate the sensor data with the complex physical models of particulate dynamics and polymer fibrillation, for the inline monitoring and control of the process. Finally, and equally excitingly, the challenges in optimising the microstructures and rheology of battery slurries are mirrored in the next-generation solar cells, where the quality of organic photovoltaic,[277] quantum dot,[62] perovskite[63] films is highly dependent on the colloidal properties of their precursor inks, which are of similarly high solid loading with polymer binders. This presents an excellent opportunity for the proposed methodology to make strong impacts on yet another renewable energy sector.

It is our firm belief that the fusion of inline ultrasonic monitoring with physics-informed predictive modelling will be instrumental to achieve closed-loop optimisation for battery slurry mixing and contiguous manufacturing processes. This review, by comprehensively outlining the problem landscape, the significant promise of ultrasound, and the key research challenges and opportunities, aims to lay a robust foundation and coordinate further research towards realising this ambitious yet critical objective for the future of energy storage technology.

Conflicts of interest

There are no conflicts to declare.

Data availability

No primary research results, software or code have been included, and no new data were generated or analysed as part of this review.

The supplementary information contains additional theoretical derivations, supporting equations, and expanded methodological explanations that complement the analyses presented in the main manuscript. See DOI: https://doi.org/10.1039/d5ee03563e.

Acknowledgements

Y. Y. gratefully acknowledges financial support from the EPSRC Centre for Doctoral Training in Future Innovation in Non-Destructive Evaluation (FIND-CDT). B. L. gratefully thanks the generous funding support from the Imperial College Non-Destructive Evaluation Group.

References

1 M. M. Thackeray, C. Wolverton and E. D. Isaacs, Electrical energy storage for transportation—approaching the limits of, and going beyond, lithium-ion batteries, *Energy Environ. Sci.*, 2012, **5**(7), 7854–7863.
2 J. Deng, C. Bae, A. Denlinger and T. Miller, Electric vehicles batteries: requirements and challenges, *Joule*, 2020, **4**(3), 511–515.
3 A. König, L. Nicoletti, D. Schröder, S. Wolff, A. Waclaw and M. Lienkamp, An overview of parameter and cost for battery electric vehicles, *World Electric Vehicle J.*, 2021, **12**(1), 21.
4 Z. Zhu, T. Jiang, M. Ali, Y. Meng, Y. Jin, Y. Cui and W. Chen, Rechargeable batteries for grid scale energy storage, *Chem. Rev.*, 2022, **122**(22), 16610–16751.

5 T. Lehtola and A. Zahedi, Solar energy and wind power supply supported by storage technology: a review, *Sustainable Energy Technol. Assess.*, 2019, **35**, 25–31.
6 G. E. Blomgren, The development and future of lithium ion batteries, *J. Electrochem. Soc.*, 2016, **164**(1), A5019.
7 M. Li, J. Lu, Z. Chen and K. Amine, 30 years of lithium-ion batteries, *Adv. Mater.*, 2018, **30**(33), 1800561.
8 T. Kim, W. Song, D.-Y. Son, L. K. Ono and Y. Qi, Lithium-ion batteries: outlook on present, future, and hybridized technologies, *J. Mater. Chem. A*, 2019, **7**(7), 2942–2964.
9 H. Fayaz, A. Afzal, A. D. Mohammed Samee, M. E. M. Soudagar, N. Akram, M. A. Mujtaba, R. D. Jilte, M. D. Tariqul Islam, Ü. Agbulut and C. Ahamed Saleel, Optimization of thermal and structural design in lithium-ion batteries to obtain energy efficient battery thermal management system (btms): a critical review, *Arch. Comput. Methods Eng.*, 2022, **29**(1), 129–194.
10 McKinsey & Company. Battery 2030: Resilient, sustainable, and circular, 2023.
11 International Energy Agency. World Energy Investment 2023 – Overview and Key Findings, 2023. Accessed: 2025-04-24.
12 Custom Market Insights. Global zinc-ion battery market size, forecast to 2030, 2022. Accessed: 14-Mar-2025.
13 Sodium Battery Hub. Sodium-ion battery market to reach usd 1.84 billion by 2030 at 21.2% growth, 2025. Accessed: 14-Mar-2025.
14 R. Berger, Battery monitor 2022: Battery production and product performance, 2022. Accessed: 21-Mar-2025.
15 G. Bockey and H. Heimes, Mastering ramp-up of battery production. Technical report, PEM of RWTH Aachen University and Fraunhofer FFB, 2024. White Paper.
16 Electric Revolution Ventures (ERV). From insight to impact: An opinion on the critical role of diagnostics in Li-ion battery production, 2024. Accessed: 21-Mar-2025.
17 S. S. Sharma and A. Manthiram, Towards more environmentally and socially responsible batteries, *Energy Environ. Sci.*, 2020, **13**(11), 4087–4097.
18 C. Baltazar Tabelin, J. Dallas, S. Casanova, T. Pelech, G. Bournival, S. Saydam and I. Canbulat, Towards a low-carbon society: a review of lithium resource availability, challenges and innovations in mining, extraction and recycling, and future perspectives, *Miner. Eng.*, 2021, **163**, 106743.
19 A. Mariele Domingues, R. G. de Souza and J. Victor Rojas Luiz, Lifecycle social impacts of lithium-ion batteries: consequences and future research agenda for a safe and just transition, *Energy Res. Soc. Sci.*, 2024, **118**, 103756.
20 A. Kwade, W. Haselrieder, R. Leithoff, A. Modlinger, F. Dietrich and K. Droeder, Current status and challenges for automotive battery production technologies, *Nat. Energy*, 2018, **3**(4), 290–300.
21 Y. Bai, M. Li, C. J. Jafta, Q. Dai, R. Essehli, B. J. Polzin and I. Belharouak, Direct recycling and remanufacturing of anode scraps, *Sustainable Mater. Technol.*, 2023, **35**, e00542.
22 L. Yu, Y. Bai, B. Polzin and I. Belharouak, Unlocking the value of recycling scrap from Li-ion battery manufacturing: challenges and outlook, *J. Power Sources*, 2024, **593**, 233955.
23 Y. Liu, R. Zhang, J. Wang and Y. Wang, Current and future lithium-ion battery manufacturing, *iScience*, 2021, **24**(4), 102332.
24 E. Ayerbe, M. Berecibar, S. Clark, A. A. Franco and J. Ruhland, Digitalization of battery manufacturing: current status, challenges, and opportunities, *Adv. Energy Mater.*, 2022, **12**(17), 2102696.
25 M. Kehrer, M. Locke, C. Offermanns, H. Heimes and A. Kampker, Analysis of possible reductions of rejects in battery cell production during switch-on and operating processes, *Energy Technol.*, 2021, **9**(7), 2001113.
26 C. D. Reynolds, H. Walker, A. Mahgoub, E. Adebayo and E. Kendrick, Battery electrode slurry rheology and its impact on manufacturing, *Energy Adv.*, 2025, **4**(1), 84–93.
27 K. W. Knehr, J. J. Kubal, P. A. Nelson and S. Ahmed. *Battery performance and cost modeling for electric-drive vehicles (a manual for batpac v5. 0). Technical report*, Argonne National Lab.(ANL), Argonne, IL (United States), 2022.
28 A. Kraytsberg and Y. Ein-Eli, Conveying advanced Li-ion battery materials into practice the impact of electrode slurry preparation skills, *Adv. Energy Mater.*, 2016, **6**(21), 1600655.
29 J. Entwistle, R. Ge, K. Pardikar, R. Smith and D. Cumming, Carbon binder domain networks and electrical conductivity in lithium-ion battery electrodes: a critical review, *Renewable Sustainable Energy Rev.*, 2022, **166**, 112624.
30 P. M. Attia, E. Moch and P. K. Herring, Challenges and opportunities for high-quality battery production at scale, *Nat. Commun.*, 2025, **16**(1), 611.
31 X. Fu, Y. Zhou, J. Huang, L. Feng, P. Yu, Q. Zhang, W. Yang and Y. Wang, Rethinking the electrode multiscale microstructures: a review on structuring strategies toward battery manufacturing genome, *Adv. Energy Mater.*, 2023, **13**(32), 2301385.
32 C. D. Reynolds, P. R. Slater, S. D. Hare, M. J. H. Simmons and E. Kendrick, A review of metrology in lithium-ion electrode coating processes, *Mater. Des.*, 2021, **209**, 109971.
33 J. Kristoffer Mayer, L. Almar, E. Asylbekov, W. Haselrieder, A. Kwade, A. Weber and H. Nirschl, Influence of the carbon black dispersing process on the microstructure and performance of Li-ion battery cathodes, *Energy Technol.*, 2020, **8**(2), 1900161.
34 M. Yousaf, U. Naseer, A. Imran, Y. Li, W. Aftab, A. Mahmood, N. Mahmood, X. Zhang, P. Gao and Y. Lu, *et al.*, Visualization of battery materials and their interfaces/interphases using cryogenic electron microscopy, *Mater. Today*, 2022, **58**, 238–274.
35 V. Wenzel, H. Nirschl and D. Nötzel, Challenges in lithium-ion-battery slurry preparation and potential of modifying electrode structures by different mixing processes, *Energy Technol.*, 2015, **3**(7), 692–698.
36 W. Blake Hawley and J. Li, Beneficial rheological properties of lithium-ion battery cathode slurries from elevated mixing and coating temperatures, *J. Energy Storage*, 2019, **26**, 100994.
37 B. Zhao, D. Yin, Y. Gao and J. Ren, Concentration dependence of yield stress, thixotropy, and viscoelasticity rheological behavior of lithium-ion battery slurry, *Ceram. Int.*, 2022, **48**(13), 19073–19080.

38 M. E. McGovern, D. D. Bruder, E. D. Huemiller, T. J. Rinker, J. T. Bracey, R. C. Sekol and J. A. Abell, A review of research needs in nondestructive evaluation for quality verification in electric vehicle lithium-ion battery cell manufacturing, *J. Power Sources*, 2023, **561**, 232742.
39 M. J. W. Povey, *Ultrasonic techniques for fluids characterization*, Elsevier, 1997.
40 R. E. Challis, M. J. W. Povey, M. L. Mather and A. K. Holmes, Ultrasound techniques for characterizing colloidal dispersions, *Rep. Progress Phys.*, 2005, **68**(7), 1541.
41 C. J. T. Sewell, Vii. The extinction of sound in a viscous atmosphere by small obstacles of cylindrical and spherical form, *Philos. Trans. R. Soc., A*, 1911, **210**(459–470), 239–270.
42 R. J. Urick and W. S. Ament, The propagation of sound in composite media, *J. Acoust. Soc. Am.*, 1949, **21**(2), 115–119.
43 M. Lax, Multiple scattering of waves, *Rev. Mod. Phys.*, 1951, **23**(4), 287.
44 P. S. Epstein and R. R. Carhart, The absorption of sound in suspensions and emulsions. I. Water fog in air, *J. Acoust. Soc. Am.*, 1953, **25**(3), 553–565.
45 J. R. Allegra and S. A. Hawley, Attenuation of sound in suspensions and emulsions: theory and experiments, *J. Acoust. Soc. Am.*, 1972, **51**(5B), 1545–1564.
46 T. A. Strout, *Attenuation of sound in high-concentration suspensions: development and application of an oscillatory cell model*, The University of Maine, 1991.
47 R. E. Challis, A. K. Holmes, J. S. Tebbutt and R. P. Cocker, Scattering of ultrasonic compression waves by particulate filler in a cured epoxy continuum, *J. Acoust. Soc. Am.*, 1998, **103**(3), 1413–1420.
48 M. Stautberg Greenwood and J. Ann Bamberger, Measurement of viscosity and shear wave velocity of a liquid or slurry for on-line process control, *Ultrasonics*, 2002, **39**(9), 623–630.
49 E. E. Franco, J. C. Adamowski, R. T. Higuti and F. Buiochi, Viscosity measurement of newtonian liquids using the complex reflection coefficient, *IEEE Trans. Ultrason. Eng.*, 2008, **55**(10), 2247–2253.
50 P. J. Coghill, M. J. Millen and B. D. Sowerby, On-line measurement of particle size in mineral slurries, *Miner. Eng.*, 2002, **15**(1–2), 83–90.
51 R. Kotze, R. Haldenwang and P. Slatter, Rheological characterization of highly concentrated mineral suspensions using ultrasound velocity profiling with combined pressure difference method, *Appl. Rheol.*, 2008, **18**(6), 62114-1.
52 D. Julian McClements and S. Gunasekaran, Ultrasonic characterization of foods and drinks: principles, methods, and applications, *Crit. Rev. Food Sci. Nutr.*, 1997, **37**(1), 1–46.
53 T. S. Awad, H. A. Moharram, O. E. Shaltout, D. Asker and M. M. Youssef, Applications of ultrasound in analysis, processing and quality control of food: a review, *Food Res. Int.*, 2012, **48**(2), 410–427.
54 G. Bonacucina, D. R. Perinelli, M. Cespi, L. Casettari, R. Cossi, P. Blasi and G. F. Palmieri, Acoustic spectroscopy: a powerful analytical method for the pharmaceutical field?, *Int. J. Pharm.*, 2016, **503**(1–2), 174–195.
55 D. Predoi, S. Liliana Iconaru, M. Valentin Predoi, M. Motelica-Heino, R. Guegan and N. Buton, Evaluation of antibacterial activity of zinc-doped hydroxyapatite colloids and dispersion stability using ultrasounds, *Nanomaterials*, 2019, **9**(4), 515.
56 T. Kusano, M. Ishii, M. Tani, O. Hiruta, T. Matsunaga and H. Nakamura, Rheological behavior of concentrated slurry and wet granules for lithium ion battery electrodes, *Adv. Powder Technol.*, 2020, **31**(11), 4491–4499.
57 Y. He, L. Jing, L. Feng, S. Yang, J. Yang, X. Fu, W. Yang and Y. Wang, A smart polymeric sol-binder for building healthy active-material microenvironment in high-energy-density electrodes, *Adv. Energy Mater.*, 2023, **13**(6), 2203272.
58 Z. Ji, L. Feng, Z. Zhu, X. Fu, W. Yang and Y. Wang, Polymeric interface engineering in lithium–sulfur batteries, *Chem. Eng. J.*, 2023, **455**, 140462.
59 X. Shen, M. Lin, Y. Shao, J.-I. Kwon and J. P.-Y. Maa, Application of ultrasonic waves to evaluate the rheological properties of non-newtonian slurries: a preliminary study, *J. Hydraulic Res.*, 2024, **62**(2), 176–191.
60 R. Kazys, L. Mazeika, R. Sliteris and R. Raisutis, Measurement of viscosity of highly viscous non-newtonian fluids by means of ultrasonic guided waves, *Ultrasonics*, 2014, **54**(4), 1104–1112.
61 G. Em Karniadakis, I. G. Kevrekidis, L. Lu, P. Perdikaris, S. Wang and L. Yang, Physics-informed machine learning, *Nat. Rev. Phys.*, 2021, **3**(6), 422–440.
62 G. H. Carey, A. L. Abdelhady, Z. Ning, S. M. Thon, O. M. Bakr and E. H. Sargent, Colloidal quantum dot solar cells, *Chem. Rev.*, 2015, **115**(23), 12732–12763.
63 D. He, P. Chen, J. A. Steele, Z. Wang, H. Xu, M. Zhang, S. Ding, C. Zhang, T. Lin and F. Kremer, *et al.*, Homogeneous 2D/3D heterostructured tin halide perovskite photovoltaics, *Nat. Nanotechnol.*, 2025, 1–8.
64 R. Tao, Y. Gu, Z. Du, X. Lyu and J. Li, Advanced electrode processing for lithium-ion battery manufacturing, *Nat. Rev. Clean Technol.*, 2025, 1–16.
65 H. Liu, X. Cheng, Y. Chong, H. Yuan, J.-Q. Huang and Q. Zhang, Advanced electrode processing of lithium ion batteries: a review of powder technology in battery fabrication, *Particuology*, 2021, **57**, 56–71.
66 G.-A. Nazri and G. Pistoia, *Lithium batteries: science and technology*, Springer Science & Business Media, 2008.
67 N. Lingappan, L. Kong and M. Pecht, The significance of aqueous binders in lithium-ion batteries, *Renewable Sustainable Energy Rev.*, 2021, **147**, 111227.
68 J. Li, J. Fleetwood, W. Blake Hawley and W. Kays, From materials to cell: state-of-the-art and prospective technologies for lithium-ion battery electrode processing, *Chem. Rev.*, 2021, **122**(1), 903–956.
69 N. Nitta, F. Wu, J. Tae Lee and G. Yushin, Li-ion battery materials: present and future, *Mater. Today*, 2015, **18**(5), 252–264.
70 M. Yoshio, R. J. Brodd and A. Kozawa, *Lithium-ion batteries*, Springer, 2009, vol. 1.
71 W. Blake Hawley and J. Li, Electrode manufacturing for lithium-ion batteries—analysis of current and next generation processing, *J. Energy Storage*, 2019, **25**, 100862.

72 W. Porcher, B. Lestriez, S. Jouanneau and D. Guyomard, Design of aqueous processed thick $LIFEPO_4$ composite electrodes for high-energy lithium battery, *J. Electrochem. Soc.*, 2008, **156**(3), A133.
73 J. Ha Chang, M. Wook Pin, I. Kim, S. Kim, S. Kim, S. Moon, J. Cho, S. Choi, B. Heo and Z. Ahmed Chandio, *et al.*, Binder migration: frequently observed yet overlooked phenomena in electrode processing for lithium-ion batteries, *J. Energy Storage*, 2024, **83**, 110729.
74 K. Huber, A. Adam, D. Grießl and A. Kwade, Understanding slurry mixing effects on the fast charging capability of lithium-ion battery cells: methodology and case study, *J. Power Sources*, 2022, **536**, 231455.
75 K. Konda, S. B. Moodakare, P. Logesh Kumar, M. Battabyal, J. R. Seth, V. A. Juvekar and R. Gopalan, Comprehensive effort on electrode slurry preparation for better electrochemical performance of $LIFEPO_4$ battery, *J. Power Sources*, 2020, **480**, 228837.
76 A. Zharbossyn, Z. Berkinova, A. Boribayeva, A. Yermukhambetova and B. Golman, Analysis of tortuosity in compacts of ternary mixtures of spherical particles, *Materials*, 2020, **13**(20), 4487.
77 Y. He, L. Jing, Y. Ji, Z. Zhu, L. Feng, X. Fu and Y. Wang, Revisiting the electrode manufacturing: a look into electrode rheology and active material microenvironment, *J. Energy Chem.*, 2022, **72**, 41–55.
78 L. Ouyang, Z. Wu, J. Wang, X. Qi, Q. Li, J. Wang and S. Lu, The effect of solid content on the rheological properties and microstructures of a Li-ion battery cathode slurry, *RSC Adv.*, 2020, **10**(33), 19360–19370.
79 R. Gordon, R. Orias and N. Willenbacher, Effect of carboxymethyl cellulose on the flow behavior of lithium-ion battery anode slurries and the electrical as well as mechanical properties of corresponding dry layers, *J. Mater. Sci.*, 2020, **55**, 15867–15881.
80 C. D. Reynolds, S. D. Hare, P. R. Slater, M. J. H. Simmons and E. Kendrick, Rheology and structure of lithium-ion battery electrode slurries, *Energy Technol.*, 2022, **10**(10), 2200545.
81 F. Font, B. Protas, G. Richardson and J. M. Foster, Binder migration during drying of lithium-ion battery electrodes: modelling and comparison to experiment, *J. Power Sources*, 2018, **393**, 177–185.
82 G. Liu, H. Zheng, S. Kim, Y. Deng, A. M. Minor, X. Song and V. S. Battaglia, Effects of various conductive additive and polymeric binder contents on the performance of a lithium-ion composite cathode, *J. Electrochem. Soc.*, 2008, **155**(12), A887.
83 S. R. Daemi, C. Tan, T. Volkenandt, S. J. Cooper, A. Palacios-Padros, J. Cookson, D. J. L. Brett and P. R. Shearing, Visualizing the carbon binder phase of battery electrodes in three dimensions, *ACS Appl. Energy Mater.*, 2018, **1**(8), 3702–3710.
84 H. Muhammad Ali, *Advances in Nanofluid Heat Transfer*, Elsevier, 2022.
85 D. Mohanty, E. Hockaday, J. Li, D. K. Hensley, C. Daniel and D. L. Wood III, Effect of electrode manufacturing defects on electrochemical performance of lithium-ion batteries: cognizance of the battery failure sources, *J. Power Sources*, 2016, **312**, 70–79.
86 N. Park, M. Lee, H. Jung and J. Nam, Complex rheological response of Li-ion battery anode slurries, *J. Power Sources*, 2024, **608**, 234607.
87 F. Ma, Y. Fu, V. Battaglia and R. Prasher, Microrheological modeling of lithium ion battery anode slurry, *J. Power Sources*, 2019, **438**, 226994.
88 J. Mewis and N. J. Wagner, Thixotropy, *Adv. Colloid Interface Sci.*, 2009, **147**, 214–227.
89 S. Lim, S. Kim, K. Hyun Ahn and S. Jong Lee, The effect of binders on the rheological properties and the microstructure formation of lithium-ion battery anode slurries, *J. Power Sources*, 2015, **299**, 221–230.
90 Y. Kim, S. Kim, B. Soo Kim, J. Hoon Park, K. Hyun Ahn and J. Dong Park, Yielding behavior of concentrated lithium-ion battery anode slurry, *Phys. Fluids*, 2022, **34**(12), 123112.
91 C. D. Reynolds, J. Lam, L. Yang and E. Kendrick, Extensional rheology of battery electrode slurries with water-based binders, *Mater. Des.*, 2022, **222**, 111104.
92 W. Jun Lee, N. Park, J. In Park, J. Nam, K. Hyun Ahn and J. Min Kim, Extensional rheology of anode slurries for Li-ion batteries containing natural and synthetic graphite, *J. Colloid Interface Sci.*, 2024, **663**, 508–517.
93 J.-H. Lee, U. Paik, V. A. Hackley and Y.-M. Choi, Effect of carboxymethyl cellulose on aqueous processing of natural graphite negative electrodes and their electrochemical performance for lithium batteries, *J. Electrochem. Soc.*, 2005, **152**(9), A1763.
94 F.-Y. Tsai, J.-H. Jhang, H.-W. Hsieh and C.-C. Li, Dispersion, agglomeration, and gelation of $LIFEPO_4$ in water-based slurry, *J. Power Sources*, 2016, **310**, 47–53.
95 N. Adachi, M. Hashiba and O. Sakurada, Rheological properties of slurries prepared using a planetary mixer, *Ceram. Int.*, 2004, **30**(6), 1055–1058.
96 J.-M. Tarascon, M. Morcrette, J. Saint, L. Aymard and R. Janot, On the benefits of ball milling within the field of rechargeable Li-based batteries, *C. R. Chim.*, 2005, **8**(1), 17–26.
97 S. Jiang, L. Xiangfeng, Z. Dunwen, W. Hongyu, L. Zhenping and X. Ruihua, A comparative study on nano La_2O_3 suspension treated by ultrasonic and ball milling, *J. Rare Earths*, 2012, **30**(11), 1116–1122.
98 E. J. Hart and A. Henglein, Free radical and free atom reactions in the sonolysis of aqueous iodide and formate solutions, *J. Phys. Chem. C*, 1985, **89**(20), 4342–4347.
99 C. Schilde, C. Mages-Sauter, A. Kwade and H. P. Schuchmann, Efficiency of different dispersing devices for dispersing nano-sized silica and alumina, *Powder Technol.*, 2011, **207**(1–3), 353–361.
100 G.-W. Lee, J. Heon Ryu, W. Han, K. Hyun Ahn and S. M. Oh, Effect of slurry preparation process on electrochemical performances of $LiCoO_2$ composite electrode, *J. Power Sources*, 2010, **195**(18), 6049–6054.
101 Z. Liu, V. Battaglia and P. P. Mukherjee, Mesoscale elucidation of the influence of mixing sequence in electrode processing, *Langmuir*, 2014, **30**(50), 15102–15113.

102 H. Zheng, L. Zhang, G. Liu, X. Song and V. S. Battaglia, Correlationship between electrode mechanics and long-term cycling performance for graphite anode in lithium ion cells, *J. Power Sources*, 2012, **217**, 530–537.
103 D. Grießl, A. Adam, K. Huber and A. Kwade, Effect of the slurry mixing process on the structural properties of the anode and the resulting fast-charging performance of the lithium-ion battery cell, *J. Electrochem. Soc.*, 2022, **169**(2), 020531.
104 D. Zapata Dominguez, J. Xu, Y. Boudjema, S. Ben Hadj Ali, F. M. Zanotto and A. A. Franco, Influence of the mixing speed in the rheology of NMC622-based Li-ion battery electrode slurries, *J. Power Sources Adv.*, 2024, **26**, 100141.
105 P. Mishra and F. Ein-Mozaffari, Critical review of different aspects of liquid-solid mixing operations, *Rev. Chem. Eng.*, 2020, **36**(5), 555–592.
106 G. R. Kasat, A. R. Khopkar, V. V. Ranade and A. Bhalchandra Pandit, CFD simulation of liquid-phase mixing in solid–liquid stirred reactor, *Chem. Eng. Sci.*, 2008, **63**(15), 3877–3885.
107 C. Zhang, J. Gu, H. Qin, Q. Xu, W. Li, X. Jia and J. Zhang, CFD analysis of flow pattern and power consumption for viscous fluids in in-line high shear mixers, *Chem. Eng. Res. Des.*, 2017, **117**, 190–204.
108 J. Xiao, F. Shi, T. Glossmann, C. Burnett and Z. Liu, From laboratory innovations to materials manufacturing for lithium-based batteries, *Nat. Energy*, 2023, **8**(4), 329–339.
109 C. Reynolds, R. Thompson and T. McLeish, Pressure and shear rate dependence of the viscosity and stress relaxation of polymer melts, *J. Rheol.*, 2018, **62**(2), 631–642.
110 F. Okkels, A. L. Østergård and M. Amin Mohammadifar, Novel method for on-line rheology measurement in manufacturing of non-newtonian liquids, *Nordic Rheol. Soc. Annu. Trans.*, 2017, **25**, 293–298.
111 D. M. Scott, Recent advances in in-process characterization of suspensions and slurries, *Powder Technol.*, 2022, **399**, 117159.
112 S. Haghi, M. Leeb, A. Molzberger and R. Daub, Measuring instruments for characterization of intermediate products in electrode manufacturing of lithium-ion batteries, *Energy Technol.*, 2023, **11**(9), 2300364.
113 H. Bockholt, W. Haselrieder and A. Kwade, Intensive powder mixing for dry dispersing of carbon black and its relevance for lithium-ion battery cathodes, *Powder Technol.*, 2016, **297**, 266–274.
114 K. Yeon Cho, Y. Il Kwon, J. Ryoun Youn and Y. Seok Song, Interaction analysis between binder and particles in multiphase slurries, *Analyst*, 2013, **138**(7), 2044–2050.
115 D. C. Orozco-Gallo, F. A. Vásquez-Arroyave and J. A. Calderón-Gutierréz, Carbon-slurry optimization for lithium-ion batteries customization, *Electrochim. Acta*, 2023, **467**, 143141.
116 H. Hagiwara, W. J. Suszynski and L. F. Francis, A Raman spectroscopic method to find binder distribution in electrodes during drying, *J. Coat. Technol. Res.*, 2014, **11**, 11–17.
117 M. Jeronimo, Q. Stewart, A. T. Weakley, J. Giacomo, X. Zhang, N. Hyslop, A. M. Dillner, M. Shupler and M. Brauer, Analysis of black carbon on filters by image-based reflectance, *Atmos. Environ.*, 2020, **223**, 117300.
118 M. Weber, J. K. Mayer and A. Kwade, The carbon black dispersion index dicb: a novel approach describing the dispersion progress of carbon black containing battery slurries, *Energy Technol.*, 2023, **11**(5), 2201299.
119 C.-C. Li and Y.-S. Lin, Interactions between organic additives and active powders in water-based lithium iron phosphate electrode slurries, *J. Power Sources*, 2012, **220**, 413–421.
120 S. Roberts, L. Chen, B. Kishore, C. E. J. Dancer, M. J. H. Simmons and E. Kendrick, Mechanism of gelation in high nickel content cathode slurries for sodium-ion batteries, *J. Colloid Interface Sci.*, 2022, **627**, 427–437.
121 B. Bitsch, J. Dittmann, M. Schmitt, P. Scharfer, W. Schabel and N. Willenbacher, A novel slurry concept for the fabrication of lithium-ion battery electrodes with beneficial properties, *J. Power Sources*, 2014, **265**, 81–90.
122 P. R. Shearing, N. P. Brandon, J. Gelb, R. Bradley, P. J. Withers, A. J. Marquis, S. Cooper and S. J. Harris, Multi length scale microstructural investigations of a commercially available Li-ion battery electrode, *J. Electrochem. Soc.*, 2012, **159**(7), A1023.
123 T. Hutzenlaub, S. Thiele, R. Zengerle and C. Ziegler, Three-dimensional reconstruction of a $LiCoO_2$ Li-ion battery cathode, *Electrochem. Solid-State Lett.*, 2011, **15**(3), A33.
124 H. Dreger, M. Huelsebrock, L. Froboese and A. Kwade, Method development for quality control of suspensions for lithium-ion battery electrodes, *Ind. Eng. Chem. Res.*, 2017, **56**(9), 2466–2474.
125 J. Wei, P. Zhang, Y. Liu, J. Liang, Y. Xia, A. Tao, K. Zhang, Z. Tie and Z. Jin, Hypersaline aqueous lithium-ion slurry flow batteries, *ACS Energy Lett.*, 2022, **7**(2), 862–870.
126 Z. Wang, T. Zhao and M. Takei, Clarification of particle dispersion behaviors based on the dielectric characteristics of cathode slurry in lithium-ion battery (LIB), *J. Electrochem. Soc.*, 2019, **166**(2), A35.
127 M. Weber, R. Moschner and A. Kwade, Modifying the network structures of high energy anodes for lithium-ion batteries through intensive dry mixing, *Energy Technol.*, 2023, **11**(5), 2200852.
128 S. Jaiser, J. Kumberg, J. Klaver, J. L. Urai, W. Schabel, J. Schmatz and P. Scharfer, Microstructure formation of lithium-ion battery electrodes during drying-an ex situ study using cryogenic broad ion beam slope-cutting and scanning electron microscopy (cryo-BIB-SEM), *J. Power Sources*, 2017, **345**, 97–107.
129 Y. Il Kwon, J. Dae Kim and Y. Seok Song, Agitation effect on the rheological behavior of lithium-ion battery slurries, *J. Electron. Mater.*, 2015, **44**, 475–481.
130 M. Müller, L. Pfaffmann, S. Jaiser, M. Baunach, V. Trouillet, F. Scheiba, P. Scharfer, W. Schabel and W. Bauer, Investigation of binder distribution in graphite anodes for lithium-ion batteries, *J. Power Sources*, 2017, **340**, 1–5.
131 R. Baddour-Hadjean and J.-P. Pereira-Ramos, Raman microspectrometry applied to the study of electrode

materials for lithium batteries, *Chem. Rev.*, 2010, **110**(3), 1278–1319.
132 K. A. Hays, B. Key, J. Li, D. L. Wood III and G. M. Veith, Si oxidation and H_2 gassing during aqueous slurry preparation for Li-ion battery anodes, *J. Phys. Chem. C*, 2018, **122**(18), 9746–9754.
133 J. Le Houx and D. Kramer, X-ray tomography for lithium ion battery electrode characterisation—a review, *Energy Rep.*, 2021, **7**, 9–14.
134 S. Dayani, H. Markötter, A. Schmidt, M. Putra Widjaja and G. Bruno, Multi-level X-ray computed tomography (XCT) investigations of commercial lithium-ion batteries from cell to particle level, *J. Energy Storage*, 2023, **66**, 107453.
135 X. Lu, A. Bertei, D. P. Finegan, C. Tan, S. R. Daemi, J. S. Weaving, K. B. O'Regan, T. M. M. Heenan, G. Hinds and E. Kendrick, *et al.*, 3d microstructure design of lithium-ion battery electrodes assisted by X-ray nano-computed tomography and modelling, *Nat. Commun.*, 2020, **11**(1), 2079.
136 S. Vierrath, L. Zielke, R. Moroni, A. Mondon, D. R. Wheeler, R. Zengerle and S. Thiele, Morphology of nanoporous carbon-binder domains in Li-ion batteries—a FIB-SEM study, *Electrochem. Commun.*, 2015, **60**, 176–179.
137 S. J. Tambio, F. Cadiou, E. Maire, N. Besnard, M. Deschamps and B. Lestriez, The concept of effective porosity in the discharge rate performance of high-density positive electrodes for automotive application, *J. Electrochem. Soc.*, 2020, **167**(16), 160509.
138 L. Bläubaum, F. Röder, C. Nowak, H. Seng Chan, A. Kwade and U. Krewer, Impact of particle size distribution on performance of lithium-ion batteries, *ChemElectroChem*, 2020, **7**(23), 4755–4766.
139 M. M. Forouzan, B. A. Mazzeo and D. R. Wheeler, Modeling the effects of electrode microstructural heterogeneities on Li-ion battery performance and lifetime, *J. Electrochem. Soc.*, 2018, **165**(10), A2127–A2144.
140 A. Tamborrino, P. Catalano and A. Leone, Using an in-line rotating torque transducer to study the rheological aspects of malaxed olive paste, *J. Food Eng.*, 2014, **126**, 65–71.
141 M. Schmitt, M. Baunach, L. Wengeler, K. Peters, P. Junges, P. Scharfer and W. Schabel, Slot-die processing of lithium-ion battery electrodes—coating window characterization, *Chem. Eng. Process.*, 2013, **68**, 32–37.
142 B. Kim, Y. Song, B. Youn and D. Lee, Dispersion homogeneity of silicon anode slurries with various binders for Li-ion battery anode coating, *Polymers*, 2023, **15**(5), 1152.
143 J. Murali Krishnan, A. P. Deshpande and P. B. Sunil Kumar, *Rheology of complex fluids*, Springer, 2010.
144 J. Kim, D. Merger, M. Wilhelm and M. E. Helgeson, Microstructure and nonlinear signatures of yielding in a heterogeneous colloidal gel under large amplitude oscillatory shear, *J. Rheol.*, 2014, **58**(5), 1359–1390.
145 M. Larsson and J. Duffy, An overview of measurement techniques for determination of yield stress, *Annu. Trans. Nord. Rheol. Soc.*, 2013, **21**, 125–138.
146 M. Dinkgreve, J. Paredes, M. M. Denn and D. Bonn, On different ways of measuring ''the'' yield stress, *J. Non-Newtonian Fluid Mech.*, 2016, **238**, 233–241.
147 I.-H. Jang, W. Jun Lee, D. Jin and J. Min Kim, Effects of flow history on extensional rheological properties of wormlike micelle solution, *RSC Adv.*, 2022, **12**(51), 32903–32911.
148 L. E. Rodd, T. P. Scott, J. J. Cooper-White and G. H. McKinley, Capillary break-up rheometry of low-viscosity elastic fluids, *Appl. Rheol.*, 2005, **15**(1), 12–27.
149 H. A. Barnes, Thixotropy—a review, *J. Non-Newtonian Fluid Mech.*, 1997, **70**(1–2), 1–33.
150 Y. Komoda, K. Ishibashi, K. Kuratani, R. Hidema, H. Suzuki and H. Kobayashi, Rheological interpretation of the structural change of LIB cathode slurry during the preparation process, *JCIS Open*, 2022, **5**, 100038.
151 P. R. Das, L. Komsiyska, O. Osters and G. Wittstock, Effect of solid loading on the processing and behavior of pedot: Pss binder based composite cathodes for lithium ion batteries, *Synth. Met.*, 2016, **215**, 86–94.
152 W. H. Herschel and R. Bulkley, Konsistenzmessungen von gummi-benzollösungen, *Kolloid-Z.*, 1926, **39**, 291–300.
153 I. M. Krieger and T. J. Dougherty, A mechanism for non-newtonian flow in suspensions of rigid spheres, *Trans. Soc. Rheol.*, 1959, **3**(1), 137–152.
154 D. Quemada, Rheology of concentrated disperse systems and minimum energy dissipation principle: I. Viscosity-concentration relationship, *Rheol. Acta*, 1977, **16**(1), 82–94.
155 T. Lombardo, J.-B. Hoock, E. N. Primo, A. C. Ngandjong, M. Duquesnoy and A. A. Franco, Accelerated optimization methods for force-field parametrization in battery electrode manufacturing modeling, *Batteries Supercaps*, 2020, **3**(8), 721–730.
156 M. Duquesnoy, T. Lombardo, F. Caro, F. Haudiquez, A. C. Ngandjong, J. Xu, H. Oularbi and A. A. Franco, Functional data-driven framework for fast forecasting of electrode slurry rheology simulated by molecular dynamics, *npj Comput. Mater.*, 2022, **8**(1), 161.
157 A. A. Potanin, R. De Rooij, D. Van den Ende and J. Mellema, Microrheological modeling of weakly aggregated dispersions, *J. Chem. Phys.*, 1995, **102**(14), 5845–5853.
158 C. Liu, T. Lombardo, J. Xu, A. C. Ngandjong and A. A. Franco, An experimentally-validated 3d electrochemical model revealing electrode manufacturing parameters' effects on battery performance, *Energy Storage Mater.*, 2023, **54**, 156–163.
159 S. H. Huang and H.-C. Zhang, Artificial neural networks in manufacturing: concepts, applications, and perspectives, *IEEE Trans. Compon., Packag., Manuf. Technol., Part A*, 1994, **17**(2), 212–228.
160 R. Pinto Cunha, T. Lombardo, E. N. Primo and A. A. Franco, Artificial intelligence investigation of NMC cathode manufacturing parameters interdependencies, *Batteries Supercaps*, 2020, **3**(1), 60–67.
161 K. Fawagreh, M. Medhat Gaber and E. Elyan, Random forests: from early developments to recent advancements, *Syst. Sci. Control Eng.*, 2014, **2**(1), 602–609.
162 K. Liu, X. Hu, H. Zhou, L. Tong, W. Dhammika Widanage and J. Marco, Feature analyses and modeling of lithium-ion battery manufacturing based on random forest classification, *IEEE/ASME Trans. Mech.*, 2021, **26**(6), 2944–2955.

163 D. J. C. MacKay, *et al.*, Introduction to Gaussian processes, *NATO ASI Ser., F*, 1998, **168**, 133–166.
164 H. Valladares, T. Li, L. Zhu, H. El-Mounayri, A. M. Hashem, A. E. Abdel-Ghany and A. Tovar, Gaussian process-based prognostics of lithium-ion batteries and design optimization of cathode active materials, *J. Power Sources*, 2022, **528**, 231026.
165 T. Lombardo, M. Duquesnoy, H. El-Bouysidy, F. Årén, A. Gallo-Bueno, P. Bjørn Jørgensen, A. Bhowmik, A. Demortière, E. Ayerbe and F. Alcaide, *et al.*, Artificial intelligence applied to battery research: hype or reality?, *Chem. Rev.*, 2021, **122**(12), 10899–10969.
166 C. Reynolds, M. Faraji Niri, M. Francis Hidalgo, R. Heymer, L. Román, G. Alsofi, H. Khanom, B. Pye, J. Marco and E. Kendrick, Impact of formulation and slurry properties on lithium-ion electrode manufacturing, *Batteries Supercaps*, 2024, **7**(2), e202300396.
167 K. Liu, Z. Wei, Z. Yang and K. Li, Mass load prediction for lithium-ion battery electrode clean production: a machine learning approach, *J. Cleaner Prod.*, 2021, **289**, 125159.
168 M. Duquesnoy, C. Liu, D. Zapata Dominguez, V. Kumar, E. Ayerbe and A. A. Franco, Machine learning-assisted multi-objective optimization of battery manufacturing from synthetic data generated by physics-based simulations, *Energy Storage Mater.*, 2023, **56**, 50–61.
169 C. Gervillié-Mouravieff, W. Bao, D. A. Steingart and Y. Shirley Meng, Non-destructive characterization techniques for battery performance and life-cycle assessment, *Nat. Rev. Electr. Eng.*, 2024, **1**(8), 547–558.
170 W. Zuo, R. Liu, J. Cai, Y. Hu, M. Almazrouei, X. Liu, T. Cui, X. Jia, E. Apodaca and J. Alami, *et al.*, Nondestructive analysis of commercial batteries, *Chem. Rev.*, 2024, **125**(1), 369–444.
171 B. Schroyen, D. Vlassopoulos, P. Van Puyvelde and J. Vermant, Bulk rheometry at high frequencies: a review of experimental approaches, *Rheol. Acta*, 2020, **59**, 1–22.
172 A. S. Dukhin and P. J. Goetz, *Characterization of liquids, nano-and microparticulates, and porous bodies using ultrasound*, Elsevier, 2010, vol. 24.
173 A. S. Dukhin and P. J. Goetz, Acoustic spectroscopy for concentrated polydisperse colloids with high density contrast, *Langmuir*, 1996, **12**(21), 4987–4997.
174 P. Mougin, D. Wilkinson, K. J. Roberts, R. Jack and P. Kippax, Sensitivity of particle sizing by ultrasonic attenuation spectroscopy to material properties, *Powder Technol.*, 2003, **134**(3), 243–248.
175 R. Weser, S. Woeckel, B. Wessely, U. Steinmann, F. Babick and M. Stintz, Ultrasonic backscattering method for in situ characterisation of concentrated dispersions, *Powder Technol.*, 2014, **268**, 177–190.
176 M. Stautberg Greenwood, Particle size and density of a slurry from ultrasonic backscattering measurements at a solid interface, *Rev. Sci. Instrum.*, 2012, **83**(9), 095101.
177 J. Huang, F. Cegla, A. Wickenden and M. Coomber, Simultaneous measurements of temperature and viscosity for viscous fluids using an ultrasonic waveguide, *Sensors*, 2021, **21**(16), 5543.
178 J. J. Faran Jr., Sound scattering by solid cylinders and spheres, *J. Acoust. Soc. Am.*, 1951, **23**(4), 405–418.
179 R. Chanamai, N. Herrmann and D. J. McClements, Influence of thermal overlap effects on the ultrasonic attenuation spectra of polydisperse oil-in-water emulsions, *Langmuir*, 1999, **15**(10), 3418–3423.
180 D. Julian McClements and M. James William Povey, Ultrasonic velocity as a probe of emulsions and suspensions, *Adv. Colloid Interface Sci.*, 1987, **27**(3–4), 285–316.
181 P. Lloyd and M. V. Berry, Wave propagation through an assembly of spheres: Iv. Relations between different multiple scattering theories, *Proc. Phys. Soc.*, 1967, **91**(3), 678.
182 J. G. Fikioris and P. C. Waterman, Multiple scattering of waves. ii. ''hole corrections'' in the scalar case, *J. Math. Phys.*, 1964, **5**(10), 1413–1420.
183 R. E. Challis and V. J. Pinfield, Ultrasonic wave propagation in concentrated slurries-the modelling problem, *Ultrasonics*, 2014, **54**(7), 1737–1744.
184 D. Julian McClements, Ultrasonic characterisation of emulsions and suspensions, *Adv. Colloid Interface Sci.*, 1991, **37**(1–2), 33–72.
185 A. K. Hipp, G. Storti and M. Morbidelli, On multiple-particle effects in the acoustic characterization of colloidal dispersions, *J. Phys. D: Appl. Phys.*, 1999, **32**(5), 568.
186 F. Luppé, J.-M. Conoir and A. N. Norris, Effective wave numbers for thermo-viscoelastic media containing random configurations of spherical scatterers, *J. Acoust. Soc. Am.*, 2012, **131**(2), 1113–1120.
187 D. Michael Forrester, J. Huang and V. J. Pinfield, Characterisation of colloidal dispersions using ultrasound spectroscopy and multiple-scattering theory inclusive of shear-wave effects, *Chem. Eng. Res. Des.*, 2016, **114**, 69–78.
188 V. J. Pinfield and D. Michael Forrester, Multiple scattering in random dispersions of spherical scatterers: effects of shear-acoustic interactions, *J. Acoust. Soc. Am.*, 2017, **141**(1), 649–660.
189 V. J. Pinfield and T. Valier-Brasier, Multi-mode multiple wave scattering in suspensions of solid particles in viscous liquids: part 1 asymptotic results, *Proc. R. Soc. A*, 2024, **480**(2292), 20240083.
190 V. J. Pinfield and T. Valier-Brasier, Multimode multiple wave scattering in suspensions of solid particles in viscous liquids: part 2: numerical validation, *Proc. R. Soc. A*, 2024, **480**(2292), 20240106.
191 J. Diarmuid Murphy, E. D. Breitenbach and H. Überall, Resonance scattering of acoustic waves from cylindrical shells, *J. Acoust. Soc. Am.*, 1978, **64**(2), 677–683.
192 M. F. Werby and G. C. Gaunaurd, Flexural resonances in obliquely insonified solid elastic spheroids, *J. Acoust. Soc. Am.*, 1989, **85**(6), 2365–2371.
193 L. W. Anson and R. C. Chivers, Ultrasonic scattering from spherical shells including viscous and thermal effects, *J. Acoust. Soc. Am.*, 1993, **93**(4), 1687–1699.
194 A. K. Hipp, G. Storti and M. Morbidelli, Acoustic characterization of concentrated suspensions and emulsions. 1. Model analysis, *Langmuir*, 2002, **18**(2), 391–404.

195 A. K. Hipp, G. Storti and M. Morbidelli, Acoustic characterization of concentrated suspensions and emulsions. 2. Experimental validation, *Langmuir*, 2002, **18**(2), 405–412.
196 R. J. Urick, The absorption of sound in suspensions of irregular particles, *J. Acoust. Soc. Am.*, 1948, **20**(3), 283–289.
197 A. H. Harker and J. A. G. Temple, Velocity and attenuation of ultrasound in suspensions of particles in fluids, *J. Phys. D: Appl. Phys.*, 1988, **21**(11), 1576.
198 R. L. Gibson Jr and M. Nafi Toksöz, Viscous attenuation of acoustic waves in suspensions, *J. Acoust. Soc. Am.*, 1989, **85**(5), 1925–1934.
199 J. M. Evans and K. Attenborough, Coupled phase theory for sound propagation in emulsions, *J. Acoust. Soc. Am.*, 1997, **102**(1), 278–282.
200 J. M. Evans and K. Attenborough, Sound propagation in concentrated emulsions: comparison of coupled phase model and core–shell model, *J. Acoust. Soc. Am.*, 2002, **112**(5), 1911–1917.
201 B. Huang, F. Fan, Y. Li and M. Su, Numerical prediction of ultrasonic attenuation in concentrated emulsions and suspensions using monte carlo method, *Ultrasonics*, 2019, **94**, 218–226.
202 S. Zhang, G. Su, H. Liu, C. Tian and M. Su, On-line measurement of particle size in high-concentration limestone slurry pipeline by monte-carlo based ultrasonic attenuation model, *Measurement*, 2024, 115007.
203 S. Zhang, G. Su, G. Niu, J. Chen and M. Su, Simultaneous measurement of particle size distribution and mixing ratio based on monte carlo ultrasonic attenuation model, *Meas. Sci. Technol.*, 2025, **36**(2), 026014.
204 R. Weser, S. Wöckel, B. Wessely and U. Hempel, Particle characterisation in highly concentrated dispersions using ultrasonic backscattering method, *Ultrasonics*, 2013, **53**(3), 706–716.
205 M. J. W. Povey, Ultrasound particle sizing: a review, *Particuology*, 2013, **11**(2), 135–147.
206 V. Stolojanu and A. Prakash, Characterization of slurry systems by ultrasonic techniques, *Chem. Eng. J.*, 2001, **84**(3), 215–222.
207 J. Ann Bamberger and M. S. Greenwood, Using ultrasonic attenuation to monitor slurry mixing in real time, *Ultrasonics*, 2004, **42**(1–9), 145–148.
208 A. A. Falola, M. Xin Huang, X. Wu Zou and X. Z. Wang, Characterization of particle size distribution in slurries using ultrasonic attenuation spectroscopy: addressing challenges of unknown physical properties, *Powder Technol.*, 2021, **392**, 394–401.
209 T. N. Hunter, J. Peakall and S. Biggs, An acoustic backscatter system for in situ concentration profiling of settling flocculated dispersions, *Miner. Eng.*, 2012, **27**, 20–27.
210 L. W. Burgess, A. M. Brodsky and P. D. Panetta, *Physical characterization of solid–liquid slurries at high weight fractions using optical and ultrasonic methods*, Technical report, Univ. of Washington, Seattle, WA (United States), 2005.
211 O. Lombard, J. Rouyer, E. Debieu, F. Blanc and E. Franceschini, Ultrasonic backscattering and microstructure in sheared concentrated suspensions, *J. Acoust. Soc. Am.*, 2020, **147**(3), 1359–1367.
212 M. Cavegn, R. Douglas, G. Akkermans and M. Kuentz, Study of an ultrasound-based process analytical tool for homogenization of nanoparticulate pharmaceutical vehicles, *J. Pharm. Sci.*, 2011, **100**(8), 3374–3385.
213 A. S. Tonge, J. Peakall, A. P. G. Lockwood, M. Barnes and T. N. Hunter, Characterizing flocculated mineral sediments with acoustic backscatter, using solid and hybrid scattering models, *Ind. Eng. Chem. Res.*, 2023, **62**(42), 17328–17342.
214 K. Tsuji, H. Nakanishi and T. Norisuye, Viscoelastic ecah: scattering analysis of spherical particles in suspension with viscoelasticity, *Ultrasonics*, 2021, **115**, 106463.
215 C. Verdier and M. Piau, Acoustic wave propagation in two-phase viscoelastic fluids: the case of polymer emulsions, *J. Acoust. Soc. Am.*, 1997, **101**(4), 1868–1876.
216 D. Aurbach, H. Teller, M. Koltypin and E. Levi, On the behavior of different types of graphite anodes, *J. Power Sources*, 2003, **119**, 2–7.
217 A. K. Hipp, G. Storti and M. Morbidelli, Particle sizing in colloidal dispersions by ultrasound. model calibration and sensitivity analysis, *Langmuir*, 1999, **15**(7), 2338–2345.
218 R. S. Al-Lashi and R. E. Challis, Ultrasonic particle sizing in aqueous suspensions of solid particles of unknown density, *J. Acoust. Soc. Am.*, 2015, **138**(2), 1023–1029.
219 A. E. Hay and A. S. Schaafsma, Resonance scattering in suspensions, *J. Acoust. Soc. Am.*, 1989, **85**(3), 1124–1138.
220 J. Landesfeind, A. Eldiven and H. A. Gasteiger, Influence of the binder on lithium ion battery electrode tortuosity and performance, *J. Electrochem. Soc.*, 2018, **165**(5), A1122–A1128.
221 W. P. Mason, W. O. Baker, H. J. McSkimin and J. H. Heiss, Measurement of shear elasticity and viscosity of liquids at ultrasonic frequencies, *Phys. Rev.*, 1949, **75**(6), 936.
222 V. Shah and K. Balasubramaniam, Effect of viscosity on ultrasound wave reflection from a solid/liquid interface, *Ultrasonics*, 1996, **34**(8), 817–824.
223 V. V. Shah and K. Balasubramaniam, Measuring newtonian viscosity from the phase of reflected ultrasonic shear wave, *Ultrasonics*, 2000, **38**(9), 921–927.
224 G. Peretti, N. Bouscharain, N. Dörr, F. Ville and R. S. Dwyer-Joyce, In situ ultrasonic viscometry of lubricants under temperature and shear, *Tribol. Int.*, 2024, **191**, 109210.
225 M. Schirru and M. Varga, A review of ultrasonic reflectometry for the physical characterization of lubricated tribological contacts: history, methods, devices, and technological trends, *Tribol. Lett.*, 2022, **70**(4), 129.
226 T. Vogt, M. J. S. Lowe and P. Cawley, Ultrasonic waveguide techniques for the measurement of material properties, *Quant. Nondestr. Eval.*, 2002, **21**, 1742–1749.
227 F. B. Cegla, P. Cawley and M. J. S. Lowe, Fluid bulk velocity and attenuation measurements in non-newtonian liquids using a dipstick sensor, *Meas. Sci. Technol.*, 2005, **17**(2), 264.
228 A. Rabani, R. E. Challis and V. J. Pinfield, The torsional waveguide viscosity probe: design and anomalous behavior, *IEEE Trans. Ultrason. Eng.*, 2011, **58**(8), 1628–1640.

229 A. Rabani, V. J. Pinfield and R. E. Challis, Rate of shear of an ultrasonic oscillating rod viscosity probe, *Ultrasonics*, 2016, **65**, 18–22.
230 W. P. Cox and E. H. Merz, Correlation of dynamic and steady flow viscosities, *J. Polym. Sci.*, 1958, **28**(118), 619–622.
231 J. Wiklund, I. Shahram and M. Stading, Methodology for in-line rheology by ultrasound Doppler velocity profiling and pressure difference techniques, *Chem. Eng. Sci.*, 2007, **62**(16), 4277–4293.
232 J. Wiklund and M. Stading, Application of in-line ultrasound Doppler-based uvp-pd rheometry method to concentrated model and industrial suspensions, *Flow Meas. Instrum.*, 2008, **19**(3–4), 171–179.
233 I. Alig, D. Lellinger, J. Sulimma and S. Tadjbakhsch, Ultrasonic shear wave reflection method for measurements of the viscoelastic properties of polymer films, *Rev. Sci. Instrum.*, 1997, **68**(3), 1536–1542.
234 X. Wang, K. V. Subramaniam and F. Lin, Ultrasonic measurement of viscoelastic shear modulus development in hydrating cement paste, *Ultrasonics*, 2010, **50**(7), 726–738.
235 A. Rabbani and D. R. Schmitt, Ultrasonic shear wave reflectometry applied to the determination of the shear moduli and viscosity of a viscoelastic bitumen, *Fuel*, 2018, **232**, 506–518.
236 J. Ophir, I. Cespedes, H. Ponnekanti, Y. Yazdi and X. Li, Elastography: a quantitative method for imaging the elasticity of biological tissues, *Ultrasonic Imaging*, 1991, **13**(2), 111–134.
237 A. P. Sarvazyan, O. V. Rudenko, S. D. Swanson, J. Brian Fowlkes and S. Y. Emelianov, Shear wave elasticity imaging: a new ultrasonic technology of medical diagnostics, *Ultrasound Med. Biol.*, 1998, **24**(9), 1419–1435.
238 S. Chen, M. Fatemi and J. F. Greenleaf, Quantifying elasticity and viscosity from measurement of shear wave speed dispersion, *J. Acoust. Soc. Am.*, 2004, **115**(6), 2781–2785.
239 S. Chen, M. W. Urban, C. Pislaru, R. Kinnick, Y. Zheng, A. Yao and J. F. Greenleaf, Shearwave dispersion ultrasound vibrometry (SDUV) for measuring tissue elasticity and viscosity, *IEEE Trans. Ultrason. Eng.*, 2009, **56**(1), 55–62.
240 S. Chen, W. Sanchez, M. R. Callstrom, B. Gorman, J. T. Lewis, S. O. Sanderson, J. F. Greenleaf, H. Xie, Y. Shi and M. Pashley, *et al.*, Assessment of liver viscoelasticity by using shear waves induced by ultrasound radiation force, *Radiology*, 2013, **266**(3), 964–970.
241 M. W. Urban, S. Chen and M. Fatemi, A review of shear-wave dispersion ultrasound vibrometry (SDUV) and its applications, *Curr. Med. Imaging*, 2012, **8**(1), 27–36.
242 N. Larcher, M. Takarli, N. Angellier, C. Petit and H. Sebbah, Towards a viscoelastic mechanical characterization of asphalt materials by ultrasonic measurements, *Mater. Struct.*, 2015, **48**, 1377–1388.
243 C. Létang, M. Piau, C. Verdier and L. Lefebvre, Characterization of wheat-flour-water doughs: a new method using ultrasound, *Ultrasonics*, 2001, **39**(2), 133–141.
244 F. Simonetti, Lamb wave propagation in elastic plates coated with viscoelastic materials, *J. Acoust. Soc. Am.*, 2004, **115**(5), 2041–2053.
245 T. J. Royston, Z. Dai, R. Chaunsali, Y. Liu, Y. Peng and R. L. Magin, Estimating material viscoelastic properties based on surface wave measurements: a comparison of techniques and modeling assumptions, *J. Acoust. Soc. Am.*, 2011, **130**(6), 4126–4138.
246 A. El Baroudi and J. Yves Le Pommellec, Viscoelastic fluid effect on the surface wave propagation, *Sens. Actuators, A*, 2019, **291**, 188–195.
247 F. Josse, F. Bender and R. W. Cernosek, Guided shear horizontal surface acoustic wave sensors for chemical and biochemical detection in liquids, *Anal. Chem.*, 2001, **73**(24), 5937–5944.
248 F. Teston, G. Feuillard, L. Tessier, L. P. Tran Hu Hue and M. Lethiecq, Analysis of the coupling between shear horizontal plate waves and liquids: application to the measurement of the shear rigidity modulus of glycerol solutions, *J. Appl. Phys.*, 2000, **87**(2), 689–694.
249 F. Simonetti and P. Cawley, On the nature of shear horizontal wave propagation in elastic plates coated with viscoelastic materials, *Proc. R. Soc. London, Ser. A*, 2004, **460**(2048), 2197–2221.
250 K. Chen, A. Yao, E. E. Zheng, J. Lin and Y. Zheng, Shear wave dispersion ultrasound vibrometry based on a different mechanical model for soft tissue characterization, *J. Ultrasound Med.*, 2012, **31**(12), 2001–2011.
251 D. Gutierrez-Lemini, *Engineering viscoelasticity*, Springer, 2014, vol. 910.
252 M. Baumgaertel and H. Henning Winter, Determination of discrete relaxation and retardation time spectra from dynamic mechanical data, *Rheol. Acta*, 1989, **28**, 511–519.
253 B. Babaei, A. Davarian, K. M. Pryse, E. L. Elson and G. M. Genin, Efficient and optimized identification of generalized Maxwell viscoelastic relaxation spectra, *J. Mech. Behav. Biomed. Mater.*, 2016, **55**, 32–41.
254 M. S. Greenwood, J. D. Adamson and L. J. Bond, Measurement of the viscosity-density product using multiple reflections of ultrasonic shear horizontal waves, *Ultrasonics*, 2006, **44**, e1031–e1036.
255 M. Huang, F. Cegla and B. Lan, Stiffness matrix method for modelling wave propagation in arbitrary multilayers, *Int. J. Eng. Sci.*, 2023, **190**, 103888.
256 A. M. R. Tayamen, S. Amsterdam and W. Chang, A model-informed analysis of battery electrodes using non-contact air-coupled ultrasound, *ChemRxiv*, 2025, preprint, DOI: 10.26434/chemrxiv-2025-957c0.
257 N. Gupta, S. Mujumdar, H. Patel, S. Masuda, N. Panwar, S. Bandyopadhyay, S. Mehta, S. Guttula, S. Afzal and R. Sharma Mittal, *et al.* Data quality for machine learning tasks, In Proceedings of the 27th ACM SIGKDD conference on knowledge discovery & data mining, 2021, pp. 4040–4041.
258 D. M. Hawkins, The problem of overfitting, *J. Chem. Inf. Comput. Sci.*, 2004, **44**(1), 1–12.
259 M. Raissi, P. Perdikaris and G. E. Karniadakis, Physics-informed neural networks: a deep learning framework for solving forward and inverse problems involving nonlinear

partial differential equations, *J. Comput. Phys.*, 2019, **378**, 686–707.

260 S. Cai, Z. Mao, Z. Wang, M. Yin and G. Em Karniadakis, Physics-informed neural networks (PINNs) for fluid mechanics: a review, *Acta Mech. Sin.*, 2021, **37**(12), 1727–1738.

261 S. Cai, Z. Wang, S. Wang, P. Perdikaris and G. Em Karniadakis, Physics-informed neural networks for heat transfer problems, *J. Heat Transfer*, 2021, **143**(6), 060801.

262 F. Wang, Z. Zhai, Z. Zhao, Y. Di and X. Chen, Physics-informed neural network for lithium-ion battery degradation stable modeling and prognosis, *Nat. Commun.*, 2024, **15**(1), 4332.

263 K. Shukla, P. Clark Di Leoni, J. Blackshire, D. Sparkman and G. Em Karniadakis, Physics-informed neural network for ultrasound nondestructive quantification of surface breaking cracks, *J. Nondestruct. Eval.*, 2020, **39**, 1–20.

264 L. Wang, H. Wang, L. Liang, J. Li, Z. Zeng and Y. Liu, Physics-informed neural networks for transcranial ultrasound wave propagation, *Ultrasonics*, 2023, **132**, 107026.

265 K. Shukla, A. D. Jagtap, J. L. Blackshire, D. Sparkman and G. Em Karniadakis, A physics-informed neural network for quantifying the microstructural properties of polycrystalline nickel using ultrasound data: a promising approach for solving inverse problems, *IEEE Signal Process. Mag.*, 2021, **39**(1), 68–77.

266 S. Cai, Z. Wang, L. Lu, T. A. Zaki and G. Em Karniadakis, DeepM&Mnet: inferring the electroconvection multiphysics fields based on operator approximation by neural networks, *J. Comput. Phys.*, 2021, **436**, 110296.

267 L. Yang, X. Meng and G. Em Karniadakis, B-PINNs: Bayesian physics-informed neural networks for forward and inverse pde problems with noisy data, *J. Comput. Phys.*, 2021, **425**, 109913.

268 N. B. Kovachkia, S. Lanthalerb and A. M. Stuartb, Operator learning, *Numer. Anal. Meets Mach. Learn.*, 2024, **25**, 419.

269 Z. Li, N. Kovachki, K. Azizzadenesheli, B. Liu, K. Bhattacharya, A. Stuart and A. Anandkumar, Fourier neural operator for parametric partial differential equations, *arXiv*, 2020, preprint, arXiv:2010.08895, DOI: 10.48550/arXiv.2010.08895.

270 Z. Li, H. Zheng, N. Kovachki, D. Jin, H. Chen, B. Liu, K. Azizzadenesheli and A. Anandkumar, Physics-informed neural operator for learning partial differential equations, *ACM/JMS J. Data Sci.*, 2024, **1**(3), 1–27.

271 Q. Cao, S. Goswami and G. Em Karniadakis, Laplace neural operator for solving differential equations, *Nat. Mach. Intell.*, 2024, **6**(6), 631–640.

272 C. Meng, S. Griesemer, D. Cao, S. Seo and Y. Liu, When physics meets machine learning: a survey of physics-informed machine learning, *Mach. Learn. Comput. Sci. Eng.*, 2025, **1**(1), 1–23.

273 Y. Lu, C.-Z. Zhao, H. Yuan, J.-K. Hu, J.-Q. Huang and Q. Zhang, Dry electrode technology, the rising star in solid-state battery industrialization, *Matter*, 2022, **5**(3), 876–898.

274 H. A. Makse, N. Gland, D. L. Johnson and L. Schwartz, Granular packings: nonlinear elasticity, sound propagation, and collective relaxation dynamics, *Phys. Rev. E: Stat., Nonlinear, Soft Matter Phys.*, 2004, **70**(6), 061302.

275 M. A. Biot, Theory of propagation of elastic waves in a fluid-saturated porous solid. I. Low-frequency range, *J. Acoust. Soc. Am.*, 1956, **28**(2), 168–178.

276 M. A. Biot, Theory of propagation of elastic waves in a fluid-saturated porous solid. II. Higher frequency range, *J. Acoust. Soc. Am.*, 1956, **28**(2), 179–191.

277 A. Holmes, E. Deniau, C. Lartigau-Dagron, A. Bousquet, S. Chambon and N. P. Holmes, Review of waterborne organic semiconductor colloids for photovoltaics, *ACS Nano*, 2021, **15**(3), 3927–3959.